Atmos. Chem. Phys., 23, 15077–15096, 2023
https://doi.org/10.5194/acp-23-15077-2023
© Author(s) 2023. This work is distributed under
the Creative Commons Attribution 4.0 License.

Atmospheric Chemistry and Physics
Open Access
EGU

Insights into secondary organic aerosol formation from the day- and nighttime oxidation of polycyclic aromatic hydrocarbons and furans in an oxidation flow reactor

Abd El Rahman El Mais[1,2], Barbara D'Anna[2], Luka Drinovec[3], Andrew T. Lambe[4], Zhe Peng[5], Jean-Eudes Petit[6], Olivier Favez[1], Selim Aït-Aïssa[1], and Alexandre Albinet[1]

[1]Ineris, Parc Technologique Alata, 60550 Verneuil-en-Halatte, France
[2]Aix Marseille Université, CNRS, LCE, 13003 Marseille, France
[3]Center for Atmospheric Research, University of Nova Gorica, 5270 Nova Gorica, Slovenia
[4]Aerodyne Research, Inc. (ARI), Billerica, Massachusetts, 01821 USA
[5]CIRES and Department of Chemistry, University of Colorado, Boulder, Colorado 80309, USA
[6]Laboratoire des Sciences du Climat et de l'Environnement (LSCE), 91190 Gif sur Yvette, France

Correspondence: Alexandre Albinet (alexandre.albinet@gmail.com, alexandre.albinet@ineris.fr)

Received: 20 June 2023 – Discussion started: 4 July 2023
Revised: 12 October 2023 – Accepted: 13 October 2023 – Published: 7 December 2023

Abstract. Secondary organic aerosols (SOAs) formed by oxidation of typical precursors largely emitted by biomass burning, such as polycyclic aromatic hydrocarbons (PAHs) and furans, are still poorly characterized. We evaluated and compared the formation yields, effective density (ρ_{eff}), absorption Ångström exponent (α), and mass absorption coefficient (MAC) of laboratory-generated SOAs from three furan compounds and four PAHs. SOAs were generated in an oxidation flow reactor under day- (OH radicals) or nighttime (NO_3 radicals) conditions. The ρ_{eff}, formation yields, α, and MAC of the generated SOAs varied depending on the precursor and oxidant considered. The ρ_{eff} of SOAs formed with OH and NO_3 tended to increase with particle size before reaching a "plateau", highlighting potential differences in SOA chemical composition and/or morphology, according to the particle size. Three times lower SOA formation yields were obtained with NO_3 compared with OH. The yields of PAH SOAs (18 %–76 %) were five to six times higher than those obtained for furans (3 %–12 %). While furan SOAs showed low or negligible light absorption properties, PAH SOAs had a significant impact in the UV–visible region, implying a significant contribution to atmospheric brown carbon. No increase in the MAC values was observed from OH to NO_3 oxidation processes, probably due to a low formation of nitrogen-containing chromophores with NO_3 only (without NO_x). The results obtained demonstrated that PAHs are significant SOA precursors emitted by biomass burning, through both, day- and nighttime processes, and have a substantial impact on the aerosol light absorption properties.

1 Introduction

Airborne particles (particulate matter, PM) have strong impacts on air quality and climate (Monks et al., 2009; Fuzzi et al., 2015; IPCC, 2022). They have also been associated with adverse health effects, including respiratory and cardiovascular diseases, mortality, and morbidity (Pope et al., 2002, 2020; Brook et al., 2010; Thurston et al., 2016; Rajagopalan et al., 2018). Biomass burning is one of the major sources of fine PM ($PM_{2.5}$) in ambient air, particularly in the winter season due to residential wood combustion (RWC) used for heating purposes (Vicente and Alves, 2018; Crippa et al., 2013; Weber et al., 2019; Zhang et al., 2019, 2020; Chen et al., 2017; Srivastava et al., 2018b; Denier van der Gon et al., 2015; G. Chen et al., 2022; Viana et al., 2016). This source also emits large amounts of volatile and semi-volatile organic compounds (VOCs and SVOCs) (Akherati et al., 2020; Bruns et al., 2016; Ahern et al., 2019; Hartikainen et al., 2018;

Rùžièková et al., 2022; Hatch et al., 2015, 2017, 2018; Baudic et al., 2016) that can undergo (photo-) chemical oxidation processes involving atmospheric oxidants, such as ozone (O_3) and hydroxyl (OH) or nitrate (NO_3) radicals, resulting in the formation of secondary organic aerosols (SOAs) (Kroll and Seinfeld, 2008; Hallquist et al., 2009; Jimenez et al., 2009; Ziemann and Atkinson, 2012; Carlton et al., 2009; Heald and Kroll, 2020). Organic aerosols constitute a significant fraction of fine PM (Bressi et al., 2021; Zhang et al., 2007, 2011), and SOAs account for a large proportion of OA (up to 90 %, depending on the location) (Zhang et al., 2007, 2011; Srivastava et al., 2018a; Kroll and Seinfeld, 2008). Identifying the major SOA precursors and investigating the physicochemical properties, formation yields, and chemical composition of SOAs are crucial to implement efficient air quality policies.

Among the different VOCs and SVOCs emitted from RWC, some have been identified as major SOA precursors, such as monoaromatic hydrocarbons (benzene, toluene, xylenes, etc.), phenols, furans, and polycyclic aromatic hydrocarbons (PAHs) (Yee et al., 2013; Bruns et al., 2016; Tiitta et al., 2016; Ahern et al., 2019; Akherati et al., 2020; Rùžièková et al., 2022). Aromatic hydrocarbons (including PAHs), oxygenated aromatic compounds (including phenolic species), and furans constitute a significant fraction of the total VOCs emitted by biomass burning (10 %–50 % (with 10 %–20 % of PAHs), 5 %–20 %, and 5 %–40 %, respectively) (Hatch et al., 2015; Schauer et al., 2001; Bruns et al., 2016; Bhattu et al., 2019). The reactivity of PAHs and furans through homogeneous (in gaseous phase) or heterogenous (gas or particle) processes with different oxidants is well documented in the literature (Keyte et al., 2013; Jiang et al., 2020; Li et al., 2018; Ringuet et al., 2012; Aschmann et al., 2011, 2014; Al Ali et al., 2022; Bierbach et al., 1995; Newland et al., 2022; Kind et al., 1996; Zheng et al., 2006). However, the level of understanding in terms of SOA formation from such species is still limited. Different studies available in the literature have been focused on the formation yields, chemical composition, and physicochemical properties of SOAs formed from PAHs and furans (Lee and Lane, 2009, 2010; Chan et al., 2009; Lee et al., 2012; Shakya and Griffin, 2010; Kleindienst et al., 2012; Zhou and Wenger, 2013a, b; Chen et al., 2016; Riva et al., 2017; Kautzman et al., 2010; Gómez Alvarez et al., 2009; Strollo and Ziemann, 2013; X. Jiang et al., 2019; Joo et al., 2019; Tajuelo et al., 2021; Srivastava et al., 2022; K. Chen et al., 2022; H. Jiang et al., 2019). However, most of these studies have been conducted with OH radicals and/or ozone, and only a small number of them have investigated the SOA formation with nitrate radicals (NO_3). While OH and O_3 are the key atmospheric oxidants during the day, NO_3 is known to be the major one during the night (Brown and Stutz, 2012). The study of NO_3 radical chemistry is crucial for describing winter pollution, when RWC is more relevant and when the night lasts longer than the day. Several authors have reported its significance in the formation of SOA from RWC emissions (Kodros et al., 2020, 2022; Jorga et al., 2021; Tiitta et al., 2016). The current underestimation of OA concentrations by air quality models by a factor of 3–5 in winter might be partly due to the neglected nighttime chemistry (Fountoukis et al., 2016; Mircea et al., 2019; Tsimpidi et al., 2014). Recent simulation results including this nighttime chemistry have shown that more than 70 % of the OAs from biomass combustion are significantly influenced by the oxidation processes that take place in the absence of light, i.e., involving the nitrate radical (Kodros et al., 2020).

Finally, atmospheric brown carbon (BrC) aerosols, which primarily absorb light in the shorter visible to the ultraviolet (UV) wavelengths, have been recognized to play a critical role in the earth's radiative balance (Hems et al., 2021; Laskin et al., 2015; Moise et al., 2015; Andreae and Gelencsér, 2006). BrC can also impact black carbon (BC) light absorption due to the so-called lensing effect under internal mixing conditions (Zhang et al., 2018; Saleh et al., 2015). On the other hand, the aging of BrC-containing OA may result in decreasing their absorptivity (Sumlin et al., 2017). Quantifying the BrC contribution to light absorption is therefore essential for an accurate interpretation of the aerosol optical depth (AOD), the atmospheric column's light extinction due to both scattering and absorption, and regional climate. Numerous studies have quantitatively characterized the parameters governing the optical absorption properties (e.g., absorption Ångström exponent (α), mass absorption coefficient (MAC), and refractive index) of SOAs formed from various biogenic and anthropogenic precursors (Lambe et al., 2013; Liu et al., 2016; Xie et al., 2017a; Dingle et al., 2019; Siemens et al., 2022; Laskin et al., 2015; H. Jiang et al., 2019; Metcalf et al., 2013; Klodt et al., 2023; He et al., 2022; K. Chen et al., 2022; Hems et al., 2021; Moise et al., 2015). However, the information regarding SOAs formed from PAHs (other than naphthalene) and furans is still far from complete (Cheng et al., 2020). Besides, as particle density is linked to optical properties due to its dominant role in the effects on refractive index, its accurate determination is crucial for the evaluation of SOA radiative forcing (Liu and Daum, 2008). Overall, density is a key physical property of particles because it influences transport properties and, thus, the fate of particles in both the atmosphere and the human respiratory system (Seinfeld and Pandis, 2016; Finlayson-Pitts and Pitts Jr, 2000).

The main objectives of this study were to evaluate and compare the formation yields, and the physical (granulometry and effective densities (ρ_{eff})) and light absorption properties (α and MAC), of the SOAs formed from typical precursors emitted by biomass burning, namely PAHs and furans following OH and NO_3-initiated oxidation and aging processes.

2 Experimental methods

2.1 Generation of radicals and SOAs using oxidation flow reactor

Most of the previous studies focusing on the SOA formation from PAHs and furans have been conducted in environmental (smog) chambers. Oxidation flow reactors (OFRs) are an alternative tool to simulate atmospheric aging (Peng and Jimenez, 2020). Several works have shown the reliability, comparability, and complementarity of the results provided using such systems in the study of SOA formation processes (Bruns et al., 2015; Peng and Jimenez, 2020). Their application in the study of SOA formation from key precursors emitted by biomass burning is of prime interest (Hodshire et al., 2019; Srivastava et al., 2022).

In our study, the stable (up to 17 h) generation of SOAs (Fig. S1 in the Supplement) has been carried out at ambient temperature ($T = 24$–$32\,^{\circ}C$) and environmentally relevant relative humidity (RH = 25 %–62 %) in a potential aerosol mass oxidation flow reactor (PAM-OFR; Aerodyne Research) (Kang et al., 2007; Lambe et al., 2011), which is a 13.3 L aluminum horizontal cylindrical chamber (46 cm long × 22 cm internal diameter (ID)) operated in a continuous flow mode (Fig. 1). Three furans (furan (99 % purity), 2-methylfuran (2-MF, 99 %), and 2,5-dimethylfuran (2,5-DMF, 99 %)), and four PAHs (naphthalene (Naph, 99 %), acenaphthylene (Acy, 75 %, and the remaining 25 % comprising acenaphthene (Ace)), phenanthrene (Phe, 99 %), and fluorene (Flu, 98 %)) have been selected as SOA precursors and studied here. All of them were obtained from Sigma Aldrich (France) and injected into the PAM-OFR in their pure state, in the absence of NO_x, and without seed particles. The injection method was determined by the state of the different substances under ambient temperature conditions. Liquid furans were injected, at a constant flow, through a 0.0152 cm ID Teflon tubing using a microliter syringe pump (TriContinent C24000; 100 µL, syringe plunger velocity of 3–17 µ steps s^{-1} (= 5.63–31.88 µL min^{-1}) depending on the compound studied and concentration generated). Then, they were subsequently nebulized or vaporized using a clean air flow of 2 L min^{-1} adjusted by a mass flow controller (MFC; MKS G series) before being introduced into the PAM-OFR. PAHs were vaporized by circulating heated clean air through a metallic tube packed with the corresponding solid compounds (50–3500 mL min^{-1}, depending on the PAH studied and concentration generated, regulated at 30 °C using a CROCO-CIL liquid chromatography column oven). A filtered air supply (TSI 3074B) combined with an air zero generator (Claind AZ air purifier 2010) were used to deliver clean, dry air and maintain the total carrier gas flow inside the PAM-OFR at 9.5 L min^{-1}.

To simulate the daytime chemistry, OH radicals were produced by photolysis of O_2 by four UV lamps emitting at $\lambda =$ 185 and 254 nm (OFR185 method) (Li et al., 2015). Briefly, the photolysis of O_2 at 185 nm produced O_3 which was then photolyzed at 254 nm to produce $O(^1D)$. $O(^1D)$ then reacted with water vapor (introduced using a Nafion membrane humidifier, FC100-80-6-MKK; Perma Pure LLC) to generate OH radicals. The lamps' voltage was set, depending on the precursor studied, between 1.8 and 3 V, and the corresponding irradiance (Ir), ranging between 6 and 126 µW cm^{-2} (Table 1) was continuously measured by the PAM-OFR photodiode (Tocon_C6, sglux). A UV photometric ozone analyzer (model 202; 2B Technologies) was used to monitor the O_3 concentrations in the PAM-OFR.

For nighttime chemistry, NO_3 radicals were generated from the thermal decomposition of N_2O_5 at room temperature in a dark OFR (OFR-iN_2O_5 method) (Lambe et al., 2020). Briefly, NO_3 and N_2O_5 were generated in the gas phase following the reaction of separate reagent flows containing approximately 100 ppm NO_2 (1 % in N_2; Air Liquide) and 200 ppm O_3 in a 152.4 cm long × 2.22 cm ID perfluoroalkoxy (PFA) laminar flow reactor (LFR) coupled to the PAM-OFR. To achieve these reagent concentrations, the NO_2 flow (1 % in N_2) was set at 20 cm^3 min^{-1}, and 2 L min^{-1} of pure O_2 (99.9995 %; Air Liquide) was passed through an ozone chamber housing a mercury fluorescent lamp. The O_3 mixing ratio inside the LFR was measured using an additional ozone analyzer (model 202; 2B Technologies). In such conditions, NO_2 concentrations in the PAM-OFR (NO_X Analyzer 42i-HL; Thermo Scientific) were below the quantification limit of 1 ppm (in the range used of 0–200 ppm).

2.2 Estimation of the injected SOA precursor concentrations

Furan and PAH concentrations introduced into the PAM-OFR were established in the range of 8–50 mg m^{-3} (3–13 ppmv) and 0.19–15.1 mg m^{-3} (0.03–3 ppmv), respectively (Tables 1 and 2). These concentrations were relatively high compared with ambient air conditions. However, they are comparable to OFR aging studies performed on biomass burning as well as solid fuel combustion emissions (Bruns et al., 2015; Budisulistiorini et al., 2021; Iaukea-Lum et al., 2022; Ortega et al., 2013; Reece et al., 2017; Zhang et al., 2021). Several previous OFR studies focusing on the SOAs from pure anthropogenic precursors, and addressing similar research questions, also have been performed with comparable high loading conditions (Lau et al., 2021; Liu et al., 2015). Besides the study of SOA formation, our objective was to further perform in vitro biological assessment (El Mais, 2023) requiring a large quantity of PM materials (collected on filters, sampling flow of 6.5 L min^{-1}; Fig. 1) similarly to various previous works (Khan et al., 2021; Offer et al., 2022; Wang et al., 2018).

Furan concentrations were calculated from the syringe pump injection flow rate, temperature, analyte molecular weight, density, and dilution ratio into the OFR carrier gas

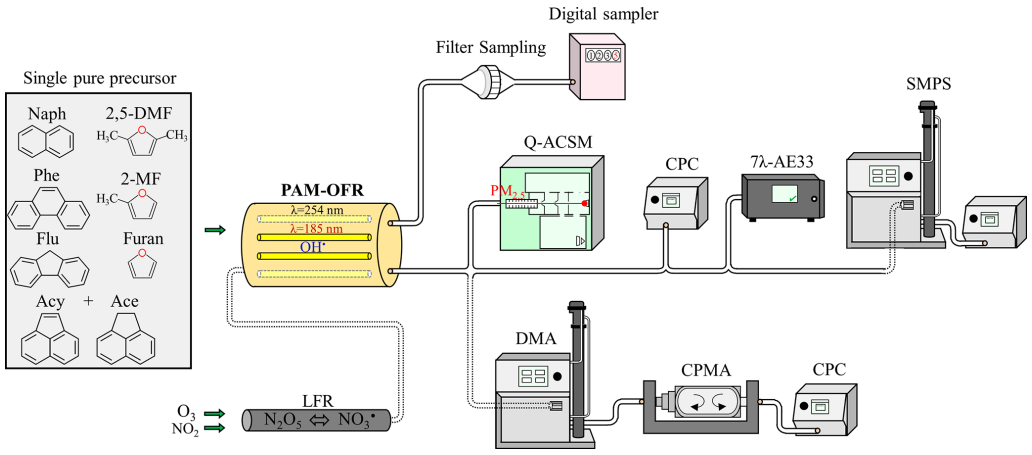

Figure 1. Simplified diagram of the experimental setup used to generate and monitor the resulting SOAs.

Table 1. Experimental conditions used to study the SOA formation from selected PAHs and furans under daytime conditions (OH radical, OFR185).

SOA precursor	SOA precursor concentration $[VOC]_0$		Voltage of the Lamps	Ir	RH	T	$[O_3]_{PAM}$	Equivalent aging days	
	($mg\,m^{-3}$)	(ppmv)	(V)	($\mu W\,cm^{-2}$)	(%)	(°C)	(ppm)	Experimental evaluation	KinSim calculations
2-methylfuran	8.99 ± 0.20	2.73 ± 0.05	3.0	71	38	30	15	6	9
2,5-dimethylfuran	17.68 ± 0.02	4.58 ± 0.01	2.8	63	38	29	12	3	6
Furan	18.41 ± 0.05	6.73 ± 0.03	2.5	34	34	29	7	n.d.*	0.1
Naphthalene	2.60 ± 0.17	0.50 ± 0.03	1.8	6	41	26	3	3	2
Acenaphthylene	0.33 ± 0.02	0.05 ± 0.00	1.8	14	39	30	4	8	12
Fluorene	0.43 ± 0.01	0.06 ± 0.00	3.0	70	39	29	11	17	20
Phenanthrene	0.19 ± 0.02	0.03 ± 0.00	3.0	58	27	29	10	11	15

* Not determined.

(Eq. S1 in the Supplement). PAH concentrations were evaluated during spare experiments under the same conditions as for SOA generation, but without oxidants (PAM-OFR lights off and no O_3 and NO_2 injected into the LFR, only O_2). Particulate and gaseous phases were collected at the PAM-OFR exit on Pallflex Tissuquartz fiber filters (Ø = 47 mm) and polyurethane foams (PUFs; 3.81×7.62 cm); Tisch Environmental), respectively. Prior to sampling, filters were preheated at 500 °C for 12 h, while PUFs were precleaned using pressurized solvent extraction (ASE 350, Thermo Scientific; one hexane cycle followed by two acetone cycles: 80 °C, 100 bars, 5 min heat time, 15 min static time) (Zielinska, 2008). Sampling durations were 15 and 30 min, and experiments were performed in duplicate for each duration. One or two experimental blanks (one for each sampling duration), for each PAH and oxidant, were also collected with no PAH injection into the PAM-OFR. After collection, samples were wrapped in aluminum foils, placed in zip bags, and then stored at −20 °C until analysis. The filter and its associated PUF (28 samples and 12 blanks in total) were extracted together using pressurized liquid extraction (ASE 200, Dionex; 80 °C, 100 bars, 5 min heat time, 15 min static time, two cycles) with acetonitrile as the solvent (VWR, high-performance liquid chromatography grade). Prior to extraction, a known amount of 6-methylchrysene was added to the samples and used as a surrogate standard to check the extraction efficiency (ranging from 88 % to 108 %). The extracts were then directly quantified (no reduction step to avoid any loss of PAH by evaporation, only a 10 times dilution was applied) by ultra-performance liquid chromatography (UPLC) fluorescence UV (Ultimate 3000; Thermo Scientific) using a C18 UPLC column (2.1 mm × 150 mm × 1.8 µm, 1 µL injected; ZORBAX Eclipse PAH; Agilent Technologies).

2.3 Online SOA characterization

The SOAs generated have been monitored and characterized using a set of different online instrumentations (Fig. 1). Organic aerosol mass and chemical composition of the non-refractory aerosol fraction were measured

Table 2. Experimental conditions used to study the SOA formation from selected PAHs and furans under nighttime conditions (NO_3 radical, OFR-iN_2O_5).

SOA precursor	SOA precursor concentration $[VOC]_0$		$[O_3]_{0,LFR}$ (ppm)	$[NO_2]_{0,LFR}$: $[O_3]_{0,LFR}$	RH (%)	T (°C)	$[O_3]_{PAM}$ (ppm)	Equivalent aging nights of 14 h
	(mg m^{-3})	(ppmv)						
2-methylfuran	41.80 ± 0.10	12.52 ± 0.02	194	0.52	49	26	11	0.1
2,5-dimethylfuran	50.23 ± 0.11	12.82 ± 0.03	179	0.56	53	25	6	0.1
Furan	18.44 ± 0.00	6.67 ± 0.00	200	0.5	62	26	10	–[a]
Naphthalene	15.10 ± 0.11	2.89 ± 0.02	194	0.51	43	25	12	5.7
Acenaphthylene	3.05 ± 0.10	0.49 ± 0.02	183	0.55	49	25	13	1.7
Fluorene	1.07 ± 0.10	0.16 ± 0.01	198	0.5	45	26	8	–[b]
Phenanthrene	0.26 ± 0.01	0.04 ± 0.00	200	0.5	43	25	10	5.6

[a] Unstable furan injection inducing an unstable SOA generation. [b] No SOA generation observed.

using a Quadrupole Aerosol Chemical Speciation Monitor (Q-ACSM; Aerodyne Research Inc.), equipped with a $PM_{2.5}$ aerodynamic lens, using a 1 min time resolution. The aerosols were dried before analysis using a Nafion dryer system. Calibration of the detector response factor was performed by using ammonium nitrate and sulfate solutions (Ng et al., 2011; Crenn et al., 2015; Freney et al., 2019). A relative ion efficiency (RIE) of 1.4 was applied to organic matter. The instrument was equipped with a capture vaporizer so that a fixed collection efficiency (CE) of 1 could be used for the whole ACSM dataset (Xu et al., 2017). Connected in parallel with the Q-ACSM, a condensation particle counter (CPC; Grimm, version 5.403), and a scanning mobility particle sizer (SMPS, composed of a differential mobility analyzer (DMA) 3081, an electrostatic classifier 3080, and a CPC 3775; TSI) were used to monitor the total particle number concentration (in the range of 4.5 nm to 3 µm, 1 s time resolution) and the particle size distribution (from 14.6 to 661.2 nm, 5 min time resolution). SOA effective density (ρ_{eff}) was evaluated by combining, in series, a DMA, a centrifugal particle mass analyzer (CPMA; Cambustion) (Olfert and Collings, 2005; Olfert et al., 2006; Johnson et al., 2013), and a CPC, all connected with the Q-ACSM (instead of the SMPS). The mass of the generated SOAs was determined for a given particle size (mobility diameter) over a range of 30–200 nm allowing the evaluation of the SOA ρ_{eff} according to the particle size. Such an approach has already been used to determine the effective density of particles of different types of primary emissions (vehicular, flame soot, etc.) and SOAs (Peng et al., 2021; Malloy et al., 2009), but only few data exist for SOAs formed from anthropogenic and biogenic precursors. Finally, a seven-wavelengths (370, 470, 520, 590, 660, 880, and 950 nm) aethalometer (1 min time resolution; AE33; Magee Scientific) was also connected at the exit of the PAM-OFR. Such an online filter tape-based optical measurement method is commonly used for the measurement of black carbon (BC) concentrations (at 880 nm) in ambient air as well as for the determination of BrC aerosol fraction (Drinovec et al., 2015, 2017; Zhang et al., 2020). Here it was used to tentatively assess SOA light absorption properties and to compare the results obtained with the most conventional techniques in the literature such as photoacoustic spectrometry or on aerosol sample extracts by UV–Vis spectroscopy (Moise et al., 2015).

2.4 Calculations

2.4.1 OH and NO_3 exposures

The OH exposure (OH_{exp}) was determined experimentally by continuously measuring the decay of SO_2 injected into the PAM-OFR (200 ppb as initial concentration) during spare experiments with the same conditions as for SOA generation, using a SO_2 analyzer (AF 21 M; Environment S.A.) (Lambe et al., 2015) and applying Eq. (1),

$$OH_{exp} = -\frac{1}{k_{SO_2}^{OH}} \times \ln\left(\frac{[SO_2]}{[SO_2]_0}\right), \quad (1)$$

where $k_{SO_2}^{OH}$ is the rate coefficient of the reaction between OH and SO_2, equal to 9.4×10^{-13} cm^3 $molecule^{-1}$ s^{-1} (Davis et al., 1979). $[SO_2]_0$ was the initial SO_2 concentration injected into the PAM-OFR, and $[SO_2]$ was the final concentration after oxidation. The OH exposure ranged from 3.74×10^{11} to 2.19×10^{12} molecules cm^{-3} s (Table S1 in the Supplement), corresponding to 3–17 equivalent aging days, respectively (Table 1), assuming a daily average OH radical concentration of 1.5×10^6 molecules cm^{-3} (Finlayson-Pitts and Pitts Jr, 2000; Mao et al., 2009).

In addition to the experimental evaluation, OH_{exp} was evaluated using the KinSim chemical kinetic solver (Peng and Jimenez, 2019). Inputs to the OFR KinSim model included pressure (P), T, RH, $[VOC]_0$ (Table 1), total residence time ($\tau = 84$ s), photon fluxes at 185 and 254 nm (I_{185} and I_{254}, respectively) (Table S2), bimolecular rate coefficients of each precursor with OH or O_3, and photoabsorption

cross sections (σ_i) of each precursor at 185 and 254 nm (Table S3).

The obtained OH_{exp} ranged from 1.05×10^{10} to 2.57×10^{12} molecules cm^{-3} s (Table S1), corresponding to about 0.1–20 equivalent aging days, and were comparable, even though larger, with the experimental values (Table 1). These differences seemed to be due to a significant rise in OH concentrations after the VOC consumption, which proportionally influenced the modeled OH_{exp} values (Fig. S2).

NO_{3exp} was estimated theoretically using a KinSim mechanism adapted from previous work (Lambe et al., 2020). Model parameters included P, T, RH, $[VOC]_0$, $[O_3]_{0,LFR}$ (Table 2), τ of 109 s, $[NO_2]$ of 100 ppm, and the bimolecular rate coefficients of each precursor with NO_3 or O_3 (Table S3). NO_{3exp} values ranged from 1.68×10^{12} to 2.10×10^{14} molecules cm^{-3} s (Table S1), corresponding to about 0.05–5.7 equivalent nights of 14 h (Table 2) at an average nighttime NO_3 mixing ratio of 7.36×10^8 molecules cm^{-3} (Asaf et al., 2010). Again, most of the NO_3 exposure was due to the modeled increase in NO_3 concentrations after VOC consumption (especially in the cases of Acy, 2-MF, and 2,5-DMF; Fig. S2).

2.4.2 Effective density

The effective density (ρ_{eff}) of SOA particles was calculated using Eq. (2) as the ratio of the measured particle mass (corresponding to the mode in the scan data (m_p)) to the calculated particle volume, assuming a spherical particle (shape factor = 1) with a diameter equal to the electrical equivalent mobility diameter (d_m) selected by the DMA (McMurry et al., 2002; DeCarlo et al., 2004):

$$\rho_{eff} = \frac{6}{\pi} \frac{m_P}{(d_m)^3}. \quad (2)$$

2.4.3 SOA yields

SOA yields were calculated using Eq. (3):

$$\text{SOA yield} = \frac{\text{mass of SOA produced}}{\text{mass of VOC reacted}}, \quad (3)$$

where the mass of VOC which reacted with the corresponding precursor was obtained from the KinSim model (see Sect. 3.1), and the mass of SOAs was determined from Q-ACSM measurements as the SOA generation was stable (Fig. S1). SOAs were considered equivalent to organic matter (OM) for OH radical experiments, and equal to $OM + NO_3$ for NO_3 radical experiments. Measurement of particle transmission through the PAM-OFR, in the range of 30–200 nm, using ammonium sulfate aerosols showed particle loss below 5 % for all PM sizes, and therefore no particle wall-loss correction was applied.

2.4.4 Optical absorption coefficient (b_{abs}), absorption Ångström exponent (α), and mass absorption coefficient (MAC)

The AE33 has been designed for automatic correction of the so-called filter loading effect (Drinovec et al., 2015, 2017). Briefly, the sampled ambient air is divided, and the sample is deposited onto two filter spots at different flow rates, leading to uneven loadings on the respective filter spots. A compensation parameter $k(\lambda)$ is retrieved from the different loading effect magnitudes influencing these two spots, and $k(\lambda)$ is further used to determine the light attenuation due to carbonaceous aerosols. However, initial results obtained, mainly for the PAH SOAs, showed a poor compensation efficiency and large jumps during the spot changes. Manual compensation of AE33 data was therefore applied using a fixed filter loading compensation parameter $k(\lambda)$ (Table S4) to get usable data (Fig. S3).

Light absorption coefficients (b_{abs}) were calculated from the manually compensated BC values according to Eq. (4):

$$b_{abs}(\lambda) = BC(\lambda) \times \sigma_{air}(\lambda) \times \frac{C_{Manufacturer}}{C_{new}}, \quad (4)$$

where σ_{air} is the air mass absorption efficiency (Table S5). Comparison between AE33 and photothermal interferometer PTAAM-2λ showed that a higher value of multiple scattering parameter C should be used (Drinovec et al., 2022) than the one provided by the manufacturer ($C_{Manufacturer} = 1.41$). A new C value (C_{new}) of 3.75 was selected for the measured particle sizes. The corrected absorption is smaller by the factor $C_{new}/C_{Manufacturer}$.

Absorption Ångström exponents (α) were determined as the absolute value of the slope of $\ln(b_{abs})$ as a function of $\ln(\lambda)$ from 370 to 590 nm. The fitting parameters are summarized in Table S6.

Mass absorption coefficients (MAC) were finally calculated as the ratio of b_{abs} to the SOA mass concentrations evaluated from Q-ACSM measurements using Eq. (5):

$$MAC(\lambda) = \frac{b_{abs}(\lambda)}{\text{SOA mass concentration}}. \quad (5)$$

3 Results and discussion

3.1 Understanding of oxidants (and photolysis) competition in the PAM-OFR for both oxidation methods

Figure 2 shows the competition between the oxidants, as well as direct photolysis, on the reactivity of the PAHs and furans studied inside the OFR.

In the case of OFR185 (OH reactivity), the predominant reaction of PAHs was observed with OH radicals (> 92 %). The remaining PAHs photolyzed at 254 nm. Both ozonolysis and photolysis at 185 nm had negligible impact on the reactivity of PAHs. For furans, photolysis at both wavelengths

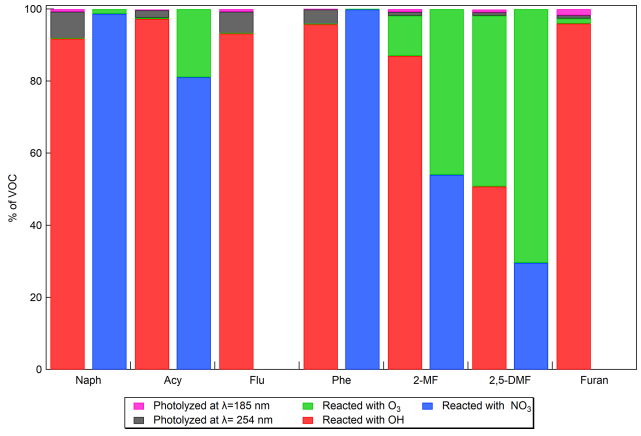

Figure 2. Relative importance of PAH and furan loss pathways inside the PAM-OFR during both OFR185 (daytime) and OFR-iN_2O_5 (nighttime) modes. No results are shown for Furan and Flu with NO_3 radicals due to an unstable SOA generation or no SOA formed.

was negligible (1 %), and the competition between OH and O_3 differed depending on the compound considered. In the case of furan, ozonolysis was negligible, and the majority (96 %) reacted with OH. This contrasted with 2-MF and 2,5-DMF, where O_3 competed with OH to consume 11 % of 2-MF and nearly half of 2,5-DMF.

In the OFR-iN_2O_5 mode (NO_3 reactivity), only O_3 and NO_3 were in competition. For Naph and Phe, O_3 had no impact. However, ozonolysis was significant for Acy (+25 % of Ace) (20 %) or even predominant for 2-MF (46 %) and 2,5-DMF (70 %).

These results showed that in our experimental conditions, the reaction with OH or NO_3 were largely the predominant ones, except for 2-MF and 2,5-DMF. These results were used to calculate the exact concentrations of the SOA precursor that reacted to get the most accurate evaluation of the SOA yields.

3.2 SOA granulometry and effective density

Figure 3 shows the average number-weighted mobility size distributions obtained for the generated SOAs under both day- and nighttime oxidation processes.

Overall, the observed particle size distributions were all monomodal and showed a shift towards larger particle sizes according to the precursor concentrations injected into the PAM-OFR. For instance, for daytime chemistry, the injected concentrations of Phe, Acy, and Flu were about 0.19–0.43 mg m^{-3}, and the resulting SOA particle distributions were centered around 32 nm, whereas the particle size distributions for Naph, 2-MF, 2,5-DMF, and furan were centered around 55 and up to 100 nm due to the larger precursor concentrations injected (2.6–18 mg m^{-3}) (Table 1). Similarly, for NO_3 radical experiments, as the precursor concentrations of Naph, Acy, and 2-MF were 4.6–10 times larger than during OH radical experiments (Table 2), a strong shift in the size distribution towards larger particles, centered around 200 nm, was observed. Interestingly, for similar precursor concentrations, the SOAs formed from Phe by reaction with NO_3 also shifted to a large particle size of about 85 nm. Moreover, the number of aerosol particles produced from Naph, Acy, Phe, and 2-MF by OH oxidation was 10–100 times larger compared with NO_3 oxidation. The aerosol particles from NO_3 oxidation grew substantially larger since fewer of them were available for semivolatiles species produced to condense onto. For 2,5-DMF, the particle size distribution shifted towards smaller particles ($D_p \sim 35$ nm), even though the concentration injected was about three times higher than during OH exposure studies. This might be also linked to the lower particle concentrations in the system observed with OH oxidation.

The effective densities of the generated SOAs with OH and NO_3 radicals as a function of the aerosol mobility diameter are presented in Fig. 4.

Generally, the SOA ρ_{eff} tended to increase with the particle size in the range of 30 to 100 or 150 nm for both reactivities. A "plateau" was then observed especially in the case of the SOAs formed by reaction with NO_3 radicals. These results highlighted potential differences in the chemical composition of the SOAs, as well as possibly in terms of their morphology, with the particle size which should be further investigated.

The average ρ_{eff} for each precursor is presented in Table 3. Values for particle diameter ≥ 100 nm were considered according to the "plateau" observed and assuming that this range of particles contributes significantly to the particle mass. Relatively large variations can be observed depending on the precursor and oxidant being studied, ranging from 1.23 to 1.61 g cm^{-3}. Between OH and NO_3 oxidation, the effective densities of Naph and Acy SOAs increased from 1.33 to 1.39 g cm^{-3} and from 1.23 to 1.47 g cm^{-3}, respectively. In contrast, the effective densities of Phe and 2-MF SOAs decreased from 1.52 to 1.29 and 1.52 to 1.38 g cm^{-3}, respectively, while they remained comparable for 2,5-DMF. The measured Naph SOA ρ_{eff} was consistent with previously reported values (1.35–1.55 g cm^{-3}) from smog chamber experiments at low and high NO_x conditions (Chan et al., 2009; Chen et al., 2016, 2018; He et al., 2022). In addition, densities of 1.24 and 1.40 g cm^{-3} have been respectively reported for 3-methylfuran SOAs (Joo et al., 2019) and furan SOAs (K. Chen et al., 2022), both formed by reaction with NO_3. Overall the values determined here were in agreement with previously reported results for SOAs formed from different anthropogenic precursors (1.06–1.65 g cm^{-3}) (Nakao et al., 2013; Kostenidou et al., 2007; Hallquist et al., 2009). In the absence of density measurements, an SOA density of 1.4 g cm^{-3} is usually assumed for smog chamber experiments (Shakya and Griffin, 2010; Riva et al., 2017; X. Jiang et al., 2019; Hallquist et al., 2009). Our results confirm this default value as a fairly good approximation, but also that it

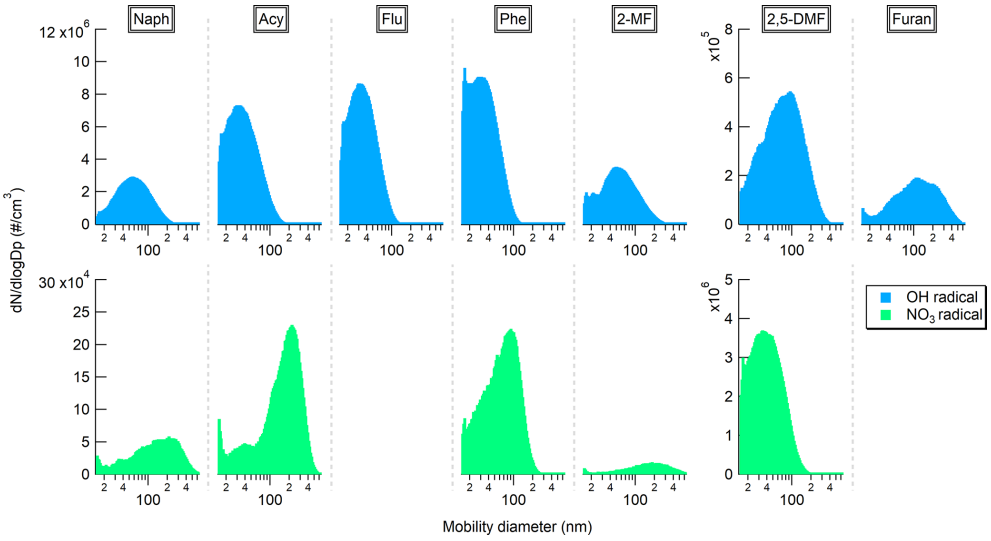

Figure 3. Comparison of the particle size distributions, in number, of the PAH and furan SOAs formed under day- and nighttime conditions (OH and NO_3 radicals, respectively). No results are shown for furan and fluorene with NO_3 radicals due to unstable SOA generation or no SOA formed.

Table 3. Average effective densities of the PAH and furan SOAs formed under day- and nighttime conditions (OH and NO_3 radicals, respectively). Results obtained from the mean of the densities corresponding to SOAs with $d_m > 100$ nm.

Precursor	Aerosol effective densities ($g\,cm^{-3}$)	
	OH radical	NO_3 radical
Naphthalene	1.33 ± 0.11	1.39 ± 0.06
Acenaphthylene	1.23 ± 0.05	1.47 ± 0.13
Fluorene	1.60 ± 0.10	No SOA formation
Phenanthrene	1.52 ± 0.02	1.29 ± 0.11
2-methylfuran	1.52 ± 0.06	1.38 ± 0.06
2,5-dimethylfuran	1.35 ± 0.08	1.35 ± 0.08
Furan	1.61 ± 0.05	Not determined

may need to be refined according to the given investigated compounds, for instance, for determining the particle transport properties, and converting PM size distributions into mass concentrations (McMurry et al., 2002). Therefore, and as reported before, our study shows the importance of figuring out the density for individual experiments to reduce the potential biases in quantitative analyses and SOA yield evaluation (Chen et al., 2016), as well as to assess the optical properties of the studied SOAs.

3.3 SOA yields

Figure 5 presents the SOA yields for the studied PAHs and furans under day- and nighttime oxidations as a function of the radical exposure used for each precursor.

The SOA yields from the oxidation of PAHs with OH radicals were all comparable, especially for Naph, Acy, and Flu, ranging from 62 % to 76 %. The differences observed, including the highest SOA yield for Phe, could be related to the differences in OH exposures ranging from 2.78×10^{11} to 2.57×10^{12} molecules cm^{-3} s (Table S1). The same has been observed for furans with comparable SOA yields (9 %–12 %), even if the range of tested OH exposures was largely variable (from 1.05×10^{10} to 1.13×10^{12} molecules cm^{-3} s. For NO_3-initiated SOA formation, approximately three times lower SOA yields were observed relative to OH-initiated SOA formation for most precursors. Only Acy showed an average SOA yield of 44 % with NO_3 comparable to that observed with OH radical chemistry (68 %), even though the NO_3 exposure tested was the lowest of the PAH group. Table 4 compares the calculated SOA yield with that of the literature. Most of the previous works reported smog chamber experiments with OH radicals, under low or high NO_X regimes and dry conditions (RH < 10 %) (Chan et al., 2009; Shakya and Griffin, 2010; Kleindienst et al., 2012; Chen et al., 2016; Riva et al., 2017; Chen et al., 2018; Gómez Alvarez et al., 2009; X. Jiang et al., 2019; Tajuelo et al., 2021). For NO_3 radicals with furan, only one previous study has reported an SOA yield of 7 % (H. Jiang et al., 2019). Joo et al. (2019) reported SOA yields of 1.6 %–2.4 % for 3-methylfuran in smog chamber dry experiments. As the experimental conditions are quite different, the reported SOA yields are also highly variable, yet our results lie on the upper range of previously reported works. Our results are two to three times higher than those of the single study performed using an OFR (Wang et al., 2018) for which no information on OH exposure is available. Several other factors influ-

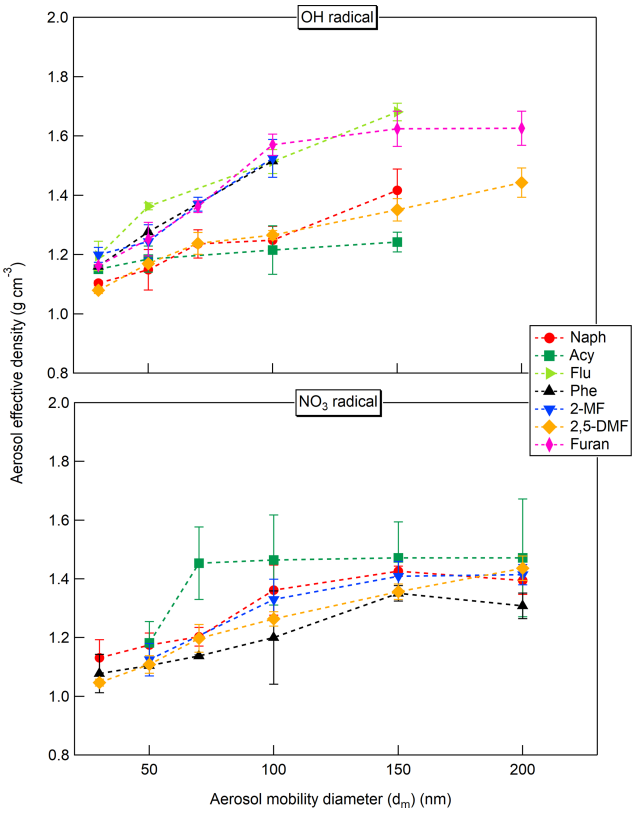

Figure 4. Comparison of the effective density of the PAH and furan SOAs formed under day- and nighttime conditions (OH and NO_3 radicals, respectively) as a function of the aerosol mobility diameter. The error bars correspond to the standard deviations ($2\,\sigma$) on the number of measurement replicates ($n = 2$–4). No results are shown for furan and fluorene with NO_3 radicals due to unstable SOA generation or no SOA formed.

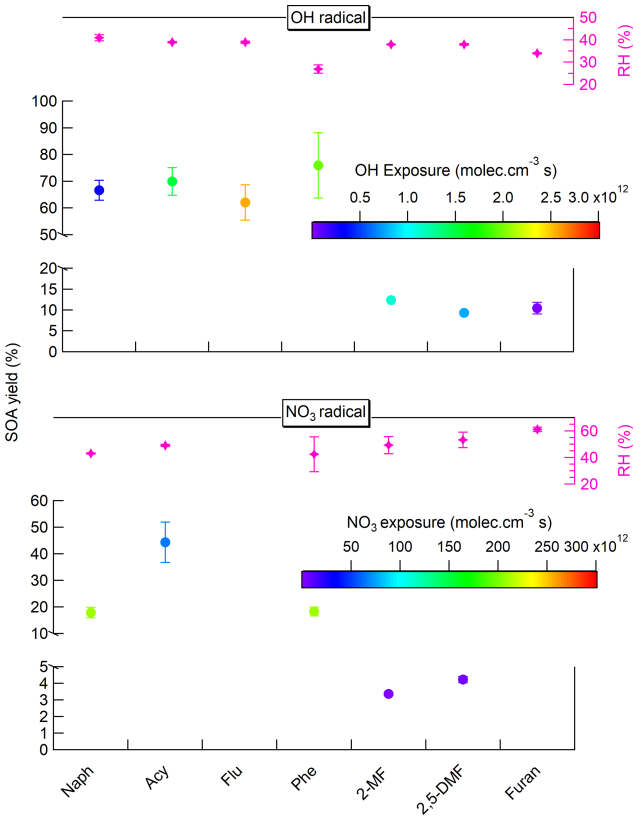

Figure 5. Comparison of the PAH and furan SOA yields obtained from the day- and nighttime oxidation processes (with OH and NO_3 radicals, respectively). Results were evaluated using Q-ACSM measurements and expressed as a function of OH or NO_3 exposures obtained from KinSim simulations. No results are shown for furan and fluorene with NO_3 radicals due to unstable SOA generation or no SOA formed.

ence the SOA yields such as the NO_x concentrations (or ratio VOC/NO_x), the use and type of seed particles, PM (organic) mass concentrations, temperature, and RH conditions (Srivastava et al., 2022; Lambe et al., 2015; Zhang et al., 2023). It has also been shown recently that smog chamber and OFR studies probably overestimate SOA formation yields compared with atmospheric conditions due to high peroxy radical (RO_2) concentrations leading to overemphasis of cross reactions of RO_2 compared with the reaction with HO_2 (or NO_3) (Schervish and Donahue, 2021). Thus, the high VOC and PM (OA) concentrations together with RH % and $RO_2 + RO_2$, $RO_2 + HO_2$ or $RO_2 + NO_3$ reaction processes may have enhanced the SOA formation here, explaining the differences observed with literature data (Table 4). Overall, SOA yields from furans oxidation were about five to six times lower than those from PAHs, implying that the contribution of furans to SOA formation from biomass burning emissions seems limited, whereas the PAH contribution is probably significant during both, day- and nighttime periods.

3.4 SOA light absorption properties (b_{abs}, α, and MAC)

Figure 6a shows the wavelength-dependent MAC values (from 370 to 590 nm) for SOAs derived from the four PAHs and three furans studied here with OH and NO_3 reactivity. A comparison with MAC values from 300 to 550 nm reported in the literature for laboratory-generated SOAs from the oxidation of furan, monoaromatic, and phenolic compounds (Lambe et al., 2013; Liu et al., 2016; Xie et al., 2017a; H. Jiang et al., 2019) is also presented. MAC values alone together with b_{abs} are shown in Fig. S4. Overall, the shape of the spectra is characteristic of atmospheric BrC materials, with higher absorption in the UV range (Laskin et al., 2015; Hems et al., 2021; Liu et al., 2016; Siemens et al., 2022; Moise et al., 2015). Our results showed significantly lower light absorption for furan SOAs than PAH SOAs for both, day- and nighttime oxidation conditions. No light absorption was observed for furan SOAs for wavelengths > 370 nm (Ångström exponents were therefore not calculated for furan SOAs). At this wavelength of 370 nm,

Table 4. Comparison of the SOA yields obtained for the different PAHs and furans studied and oxidation conditions (using the PAM-OFR) with values reported in the literature and experimental conditions specified.

SOA precursor	Experimental conditions	PM mass ($\mu g\,m^{-3}$)	SOA yield (%)	References
Naphthalene	OH, PAM-OFR, RH = 41 %	1473–1973	61.5–69.9	This study
	NO_3, PAM-OFR, RH = 43 %	2347–2911	15.7–19.5	This study
	OH, smog chamber, low NO_x, 5 % < RH < 8 %, seed	10–29	73	Chan et al. (2009)
	OH, smog chamber, high NO_x, 5 % < RH < 8 %, seed	8–28	19–30	Chan et al. (2009)
	OH, smog chamber, low NO_x, RH < 5 %	4–18	8–16	Shakya and Griffin (2010)
	OH, smog chamber, low NO_x, RH < 3 %, seed	22–158	18–36	Kleindienst et al. (2012)
	OH, smog chamber, high NO_x, RH = 30 %, seed	39–132	11–29	Kleindienst et al. (2012)
	OH, smog chamber, low NO_x, RH < 0.1 %	6–50	4–31	Chen et al. (2016)
	OH, smog chamber, high NO_x, RH < 0.1 %	3–95	3–60	Chen et al. (2016)
	OH, smog chamber, low NO_x, RH < 0.1 %	40–80	21–50	Chen et al. (2018)
	OH, OFR, RH = 57 %	Not indicated	28 ± 6.7	Wang et al. (2018)
Acenaphthylene	OH, PAM-OFR, RH = 39 %	557–1340	62.4–78.2	This study
	NO_3, PAM-OFR, RH = 49 %	1177–1502	39.0–49.8	This study
	OH, smog chamber, low NO_x, RH < 5 %	1–15	4–13	Shakya and Griffin (2010)
	OH, smog chamber, low NO_x, RH < 1 %	1120	61	Riva et al. (2017)
	OH, smog chamber, high NO_x, RH < 1 %	730	46	Riva et al. (2017)
Fluorene	OH, PAM-OFR, RH = 39 %	174–331	54.9–67.9	This study
Phenanthrene	OH, PAM-OFR, RH = 27 %	108–161	59.1–88.1	This study
	NO_3, PAM-OFR, RH = 43 %	44–53	16.7–20.1	This study
	OH, OFR, RH = 57 %	Not indicated	12 ± 2.6	Wang et al. (2018)
2-methylfuran	OH, PAM-OFR, RH = 38 %	500–985	12.3–12.5	This study
	NO_3, PAM-OFR, RH = 49 %	739–899	3.3–3.5	This study
	OH, smog chamber, high NO_x, dry conditions	13	5.5 ± 1.6	Gómez Alvarez et al. (2009)
2,5-dimethylfuran	OH, PAM-OFR, RH = 38 %	810–884	9.0–9.8	This study
	NO_3, PAM-OFR, RH = 53 %	598–721	4.0–4.4	This study
	OH, smog chamber, 25 % < RH < 60 %	4–15	0.4–6.2	Tajuelo et al. (2021)
	OH, smog chamber, high NO_x, RH < 10 %	2	0.9–1.2	Tajuelo et al. (2021)
Furan	OH, PAM-OFR, RH = 34 %	1667–2030	9.4–11.5	This study
	OH, smog chamber, high NO_x, 5 % < RH < 88 %, seed	1–119	0.04–5	X. Jiang et al. (2019)
	OH, smog chamber, high NO_x, dry conditions	69–74	1.9–7.2	Gómez Alvarez et al. (2009)
	NO_3, smog chamber, RH = 2 %–16 %	17–47	7	H. Jiang et al. (2019)

the highest MAC value was observed for Acy with OH radicals ($0.97 \pm 0.06\,m^2\,g^{-1}$). Other PAH SOAs generated with OH radicals showed comparable MAC values in the range of 0.36–0.44 $m^2\,g^{-1}$. Several studies have reported MAC values for Naph SOAs, at 400–405 nm, in the range of 0.02–0.35 $m^2\,g^{-1}$ with low NO_x (Table S7) (Updyke et al., 2012; Lambe et al., 2013; Lee et al., 2014; Xie et al., 2017a; Siemens et al., 2022; Metcalf et al., 2013; Klodt et al., 2023; He et al., 2022). Results at 400 nm, with an average MAC value of 0.22 $m^2\,g^{-1}$, were in good agreement with the literature data obtained from filter extracts. The same applies to the absorption Ångström exponent (α) for which the value of 5.43 ± 0.15 obtained was comparable to that of the literature data (ranging from 5.2 to 8.9). These results show that the filter tape-based optical method (aethalometer) applied here can provide a good estimate of such aerosol optical properties. However, using AE33 data, the characterization of the UV region is limited to 370 nm, whereas major light absorption for SOAs has been mainly reported from 350 nm and below.

Over the PAH SOAs formed with OH radicals, Naph showed the lowest α value (Fig. S5). Acy SOAs had the highest α of 8.35 ± 0.25, while Phe and Flu SOAs showed comparable values (6.92 ± 0.48 and 6.08 ± 0.51, respectively). With NO_3, the α values for Naph (5.57 ± 0.12) and Phe SOAs (7.05 ± 0.88) were similar as with OH reactivity, whereas a significantly lower α value was obtained for Acy (6.78 ± 0.13), which was comparable to that of Phe. Similarly, the MAC value (at 370 nm) of Acy SOAs formed with NO_3 radicals ($0.41 \pm 0.12\,m^2\,g^{-1}$) was largely lower than with the OH radicals and comparable to Phe ($0.43 \pm 0.10\,m^2\,g^{-1}$) and, to a lesser extent, to Naph SOAs ($0.32 \pm 0.03\,m^2\,g^{-1}$). The MAC values for furan SOAs were significantly lower and about $0.010\,m^2\,g^{-1}$ for 2-MF, 2,5-

DMF, and furan with OH radicals, and ranging from 0.005 to 0.021 $m^2\ g^{-1}$ for 2-MF and 2,5-DMF with NO_3 radicals. A similar range has been reported for furan SOAs formed by oxidation with NO_3 radicals (0.08–0.11 $m^2\ g^{-1}$) (H. Jiang et al., 2019; K. Chen et al., 2022). While furan SOAs exhibit a low light absorption in the UV region, PAH SOAs absorption properties are significant. Only m-cresol and benzene SOAs formed under high NO_x concentrations show higher MAC values in the UV–visible region (Fig. 6a). MAC values determined here are comparable to those from ambient air biomass burning organic aerosols (BBOA) (Fig. 6b) (Moise et al., 2015; Hoffer et al., 2006; Lack et al., 2012; Washenfelder et al., 2015; Zhang et al., 2016; Xie et al., 2017b; Cappa et al., 2019; Soleimanian et al., 2020; Mbengue et al., 2021). PAH emissions from biomass burning (except naphthalene, which is in the same range) are about 4 to 10 times lower than those of benzene, toluene, phenol, or furans, and are comparable to other monoaromatics and phenolic species (Bruns et al., 2016; Schauer et al., 2001; Bhattu et al., 2019; Hatch et al., 2015). Considering the SOA formation yields of these species and their contribution to the total SOA produced from biomass burning emissions (Bruns et al., 2016) (e.g., comparable for naphthalene and benzene, twice lower for phenol, and four times higher for m-cresol), and considering the light absorption properties of the different SOAs (Fig. 6), we can deduce that PAH SOAs are a significant BrC component of the emissions following biomass burning.

Finally, MAC values obtained for PAH and furan SOAs with NO_3 radicals were either similar to values observed with OH radicals, or even lower (i.e., for Acy SOAs). Only NO_3 radicals with 2,5-DMF gave higher MAC values. Usually, higher light absorption values are observed for anthropogenic SOAs formed under a high NO_x regime due to the formation of stronger nitrogen-containing chromophores (nitroaromatic mainly) (Moise et al., 2015; Hems et al., 2021; He et al., 2022; Liu et al., 2016; Klodt et al., 2023; Laskin et al., 2015; Siemens et al., 2022; Xie et al., 2017a). The SOA formation with NO_3 radical alone does not induce necessarily a large formation of nitro-organic species. For PAHs, a significant formation of nitro-chromophore species is usually observed upon heterogeneous oxidation processes with NO_3 radicals (gas or particle) but not for homogeneous reactions in the gaseous phase (Cheng et al., 2020; Kwamena and Abbatt, 2008; Lu et al., 2011; Keyte et al., 2013). Once the aerosols form in the PAM-OFR, heterogeneous reactions may occur, but reactions involving NO_3 interaction with substituent groups through H-atom abstraction, for example, for Ace, Acy, and Flu, are not expected to induce an addition of NO_2 on the by-products formed (Keyte et al., 2013; Zhou and Wenger, 2013a, b). The reaction of Naph with NO_3 alone induces a formation of nitronaphthalenes and nitronaphthols (Keyte et al., 2013) that are mainly in the gaseous phase (two-ring compounds) (Tomaz et al., 2016; Nalin et al., 2016; Reisen et al., 2003) and are not associated with the SOAs formed.

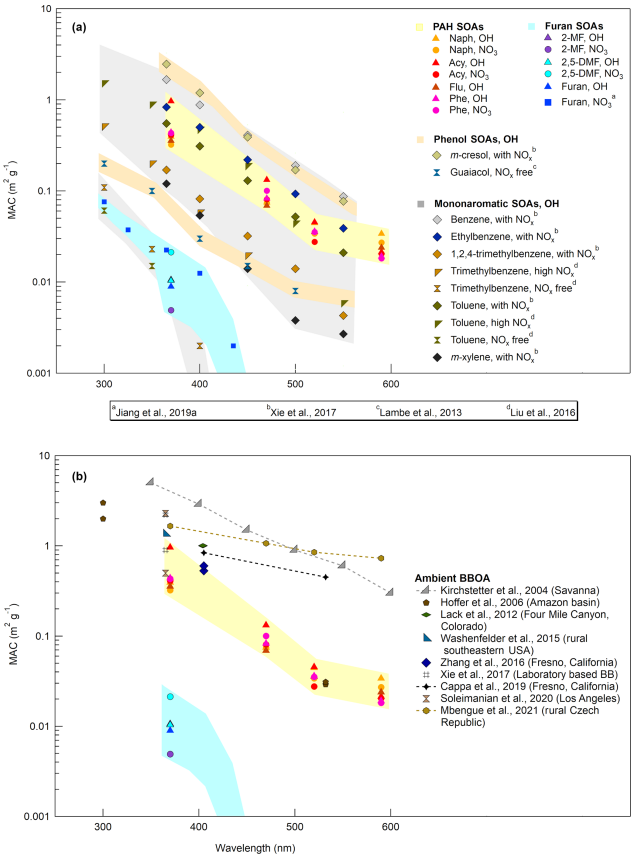

Figure 6. Comparison of the mass absorption cross section (MAC) from the day- and nighttime oxidation processes (with OH and NO_3 radicals, respectively) with literature data for laboratory-generated SOAs from anthropogenic precursors **(a)** and with data for ambient air biomass burning organic aerosols (BBOA) **(b)**.

4 Conclusions

The understanding of the formation processes and physicochemical properties of the SOAs formed from the oxidation of typical SOA precursors emitted by biomass burning, such as PAHs and furans is still limited. This study provides new key information on the properties of such SOAs formed under both, day- and nighttime chemistry. PAH SOA formation yields were five to six times greater than those evaluated for furans (3 %–12 %), illustrating the significant potential of PAHs in terms of SOA formation. Under our conditions, without NO_x, the SOA yields observed with NO_3 radicals were three times lower than with OH. The SOA formation yields obtained here from OFR experiments were either consistent with or higher than those reported in previous studies, essentially from environmental (smog) chamber experiments. This might be the result of the different experimental conditions applied in terms of oxidant, SOA precursor, PM (OA) mass or NO_x concentrations, cross reactions of RO_2, and humidity. One main limitation of this work is related to the high loadings used, and the results obtained should

be refined by experiments performed in conditions closer to ambient air conditions. However, our results showed again that OFR is a relevant alternative and complementary tool to smog chambers to simulate atmospheric aging (Bruns et al., 2015; Peng and Jimenez, 2020). The SOA effective density showed an increasing trend with particle size for both reactivities before reaching a "plateau", highlighting potential differences in terms of chemical composition and morphology with the particle size. As this was not expected, and it is still not fully understood, further works are needed to study such behavior of the SOAs formed by nucleation processes. PAH SOAs showed a higher light absorption in the range of 370–590 nm in comparison with furans that do not show significant absorption at wavelengths higher than 370 nm. Such results demonstrate that PAH SOAs can contribute significantly to ambient air BrC linked to biomass burning emissions. Finally, no increase in the MAC values was observed from OH to NO_3 oxidation processes, probably due to a low formation of nitrogen-containing chromophores with NO_3 only (without NO_x). As it is well known that NO_x has a significant impact on SOA formation (in terms of yields, for instance) and their optical properties, with the subsequent formation of strong absorbing chromophores, experiments performed under high NO_x conditions, with both OH and NO_3 radicals, will be the focus of future work. Overall, the results obtained in this study are of key importance to improve air quality and climate models.

Data availability. Data are available upon request to the authors.

Supplement. The supplement related to this article is available online at: https://doi.org/10.5194/acp-23-15077-2023-supplement.

Author contributions. AA designed and led the research. AEM and AA performed the experiments. AEM and AA analyzed the data. AEM, AA, BD, ZP, OF, JEP, LD, and ATL contributed to the interpretation of the data and results. AA was responsible for funding acquisition. AA, SAA, and BD supervised AEM's PhD work. AEM and AA wrote the manuscript with input from all co-authors.

Competing interests. The contact author has declared that none of the authors has any competing interests.

Disclaimer. Publisher's note: Copernicus Publications remains neutral with regard to jurisdictional claims made in the text, published maps, institutional affiliations, or any other geographical representation in this paper. While Copernicus Publications makes every effort to include appropriate place names, the final responsibility lies with the authors.

Acknowledgements. The authors gratefully acknowledge Serguei Stavrovski, Ahmad El Masri, Robin Aujay, Nicolas Karoski, Tanguy Amodeo, and Laurent Meunier (Ineris) for their help with the different instrumentations and for sample preparation and PAH analyses.

Financial support. This work has been supported by the French Ministry of the Environment.

Review statement. This paper was edited by Arthur Chan and reviewed by four anonymous referees.

References

Ahern, A. T., Robinson, E. S., Tkacik, D. S., Saleh, R., Hatch, L. E., Barsanti, K. C., Stockwell, C. E., Yokelson, R. J., Presto, A. A., Robinson, A. L., Sullivan, R. C., and Donahue, N. M.: Production of Secondary Organic Aerosol During Aging of Biomass Burning Smoke From Fresh Fuels and Its Relationship to VOC Precursors, J. Geophys. Res.-Atmos., 124, 3583–3606, https://doi.org/10.1029/2018JD029068, 2019.

Akherati, A., He, Y., Coggon, M. M., Koss, A. R., Hodshire, A. L., Sekimoto, K., Warneke, C., de Gouw, J., Yee, L., Seinfeld, J. H., Onasch, T. B., Herndon, S. C., Knighton, W. B., Cappa, C. D., Kleeman, M. J., Lim, C. Y., Kroll, J. H., Pierce, J. R., and Jathar, S. H.: Oxygenated Aromatic Compounds are Important Precursors of Secondary Organic Aerosol in Biomass-Burning Emissions, Environ. Sci. Technol., 54, 8568–8579, https://doi.org/10.1021/acs.est.0c01345, 2020.

Al Ali, F., Coeur, C., Houzel, N., Bouya, H., Tomas, A., and Romanias, M. N.: Rate Coefficients for the Gas-Phase Reactions of Nitrate Radicals with a Series of Furan Compounds, J. Phys. Chem. A, 126, 8674–8681, https://doi.org/10.1021/acs.jpca.2c03828, 2022.

Andreae, M. O. and Gelencsér, A.: Black carbon or brown carbon? The nature of light-absorbing carbonaceous aerosols, Atmos. Chem. Phys., 6, 3131–3148, https://doi.org/10.5194/acp-6-3131-2006, 2006.

Asaf, D., Tas, E., Pedersen, D., Peleg, M., and Luria, M.: Long-Term Measurements of NO_3 Radical at a Semiarid Urban Site: 2. Seasonal Trends and Loss Mechanisms, Environ. Sci. Technol., 44, 5901–5907, https://doi.org/10.1021/es100967z, 2010.

Aschmann, S. M., Nishino, N., Arey, J., and Atkinson, R.: Kinetics of the Reactions of OH Radicals with 2- and 3-Methylfuran, 2,3- and 2,5-Dimethylfuran, and E - and Z -3-Hexene-2,5-dione, and Products of OH + 2,5-Dimethylfuran, Environ. Sci. Technol., 45, 1859–1865, https://doi.org/10.1021/es103207k, 2011.

Aschmann, S. M., Nishino, N., Arey, J., and Atkinson, R.: Products of the OH Radical-Initiated Reactions of Furan, 2- and 3-Methylfuran, and 2,3- and 2,5-Dimethylfuran in the Presence of NO, J. Phys. Chem. A, 118, 457–466, https://doi.org/10.1021/jp410345k, 2014.

Baudic, A., Gros, V., Sauvage, S., Locoge, N., Sanchez, O., Sarda-Estève, R., Kalogridis, C., Petit, J.-E., Bonnaire, N., Baisnée, D., Favez, O., Albinet, A., Sciare, J., and Bonsang, B.: Seasonal variability and source apportionment of volatile organic com-

pounds (VOCs) in the Paris megacity (France), Atmos. Chem. Phys., 16, 11961–11989, https://doi.org/10.5194/acp-16-11961-2016, 2016.

Bhattu, D., Zotter, P., Zhou, J., Stefenelli, G., Klein, F., Bertrand, A., Temime-Roussel, B., Marchand, N., Slowik, J. G., Baltensperger, U., Prévôt, A. S. H., Nussbaumer, T., El Haddad, I., and Dommen, J.: Effect of Stove Technology and Combustion Conditions on Gas and Particulate Emissions from Residential Biomass Combustion, Environ. Sci. Technol., 53, 2209–2219, https://doi.org/10.1021/acs.est.8b05020, 2019.

Bierbach, A., Barnes, I., and Becker, K. H.: Product and kinetic study of the OH-initiated gas-phase oxidation of Furan, 2-methylfuran and furanaldehydes at 300 K, Atmos. Environ., 29, 2651–2660, https://doi.org/10.1016/1352-2310(95)00096-H, 1995.

Bressi, M., Cavalli, F., Putaud, J. P., Fröhlich, R., Petit, J.-E., Aas, W., Äijälä, M., Alastuey, A., Allan, J. D., Aurela, M., Berico, M., Bougiatioti, A., Bukowiecki, N., Canonaco, F., Crenn, V., Dusanter, S., Ehn, M., Elsasser, M., Flentje, H., Graf, P., Green, D. C., Heikkinen, L., Hermann, H., Holzinger, R., Hueglin, C., Keernik, H., Kiendler-Scharr, A., Kubelová, L., Lunder, C., Maasikmets, M., Makeš, O., Malaguti, A., Mihalopoulos, N., Nicolas, J. B., O'Dowd, C., Ovadnevaite, J., Petralia, E., Poulain, L., Priestman, M., Riffault, V., Ripoll, A., Schlag, P., Schwarz, J., Sciare, J., Slowik, J., Sosedova, Y., Stavroulas, I., Teinemaa, E., Via, M., Vodièka, P., Williams, P. I., Wiedensohler, A., Young, D. E., Zhang, S., Favez, O., Minguillón, M. C., and Prevot, A. S. H.: A European aerosol phenomenology – 7: High-time resolution chemical characteristics of submicron particulate matter across Europe, Atmos. Environ.: X, 10, 100108, https://doi.org/10.1016/j.aeaoa.2021.100108, 2021.

Brook, R. D., Rajagopalan, S., Pope, C. A., Brook, J. R., Bhatnagar, A., Diez-Roux, A. V., Holguin, F., Hong, Y., Luepker, R. V., Mittleman, M. A., Peters, A., Siscovick, D., Smith, S. C., Whitsel, L., and Kaufman, J. D.: Particulate Matter Air Pollution and Cardiovascular Disease, Circulation, 121, 2331–2378, https://doi.org/10.1161/CIR.0b013e3181dbece1, 2010.

Brown, S. S. and Stutz, J.: Nighttime radical observations and chemistry, Chem. Soc. Rev., 41, 6405–6447, https://doi.org/10.1039/C2CS35181A, 2012.

Bruns, E. A., El Haddad, I., Keller, A., Klein, F., Kumar, N. K., Pieber, S. M., Corbin, J. C., Slowik, J. G., Brune, W. H., Baltensperger, U., and Prévôt, A. S. H.: Inter-comparison of laboratory smog chamber and flow reactor systems on organic aerosol yield and composition, Atmos. Meas. Tech., 8, 2315–2332, https://doi.org/10.5194/amt-8-2315-2015, 2015.

Bruns, E. A., El Haddad, I., Slowik, J. G., Kilic, D., Klein, F., Baltensperger, U., and Prévôt, A. S. H.: Identification of significant precursor gases of secondary organic aerosols from residential wood combustion, Sci. Rep., 6, 27881, https://doi.org/10.1038/srep27881, 2016.

Budisulistiorini, S. H., Chen, J., Itoh, M., and Kuwata, M.: Can Online Aerosol Mass Spectrometry Analysis Classify Secondary Organic Aerosol (SOA) and Oxidized Primary Organic Aerosol (OPOA)? A Case Study of Laboratory and Field Studies of Indonesian Biomass Burning, ACS Earth Space Chem., 5, 3511–3522, https://doi.org/10.1021/acsearthspacechem.1c00319, 2021.

Cappa, C. D., Zhang, X., Russell, L. M., Collier, S., Lee, A. K. Y., Chen, C.-L., Betha, R., Chen, S., Liu, J., Price, D. J., Sanchez, K. J., McMeeking, G. R., Williams, L. R., Onasch, T. B., Worsnop, D. R., Abbatt, J., and Zhang, Q.: Light Absorption by Ambient Black and Brown Carbon and its Dependence on Black Carbon Coating State for Two California, USA, Cities in Winter and Summer, J. Geophys. Res.-Atmos., 124, 1550–1577, https://doi.org/10.1029/2018JD029501, 2019.

Carlton, A. G., Wiedinmyer, C., and Kroll, J. H.: A review of Secondary Organic Aerosol (SOA) formation from isoprene, Atmos. Chem. Phys., 9, 4987–5005, https://doi.org/10.5194/acp-9-4987-2009, 2009.

Chan, A. W. H., Kautzman, K. E., Chhabra, P. S., Surratt, J. D., Chan, M. N., Crounse, J. D., Kürten, A., Wennberg, P. O., Flagan, R. C., and Seinfeld, J. H.: Secondary organic aerosol formation from photooxidation of naphthalene and alkylnaphthalenes: implications for oxidation of intermediate volatility organic compounds (IVOCs), Atmos. Chem. Phys., 9, 3049–3060, https://doi.org/10.5194/acp-9-3049-2009, 2009.

Chen, C.-L., Kacarab, M., Tang, P., and Cocker, D. R.: SOA formation from naphthalene, 1-methylnaphthalene, and 2-methylnaphthalene photooxidation, Atmos. Environ., 131, 424–433, https://doi.org/10.1016/j.atmosenv.2016.02.007, 2016.

Chen, C.-L., Li, L., Tang, P., and Cocker, D. R.: SOA formation from photooxidation of naphthalene and methylnaphthalenes with m-xylene and surrogate mixtures, Atmos. Environ., 180, 256–264, https://doi.org/10.1016/j.atmosenv.2018.02.051, 2018.

Chen, G., Canonaco, F., Tobler, A., Aas, W., Alastuey, A., Allan, J., Atabakhsh, S., Aurela, M., Baltensperger, U., Bougiatioti, A., De Brito, J. F., Ceburnis, D., Chazeau, B., Chebaicheb, H., Daellenbach, K. R., Ehn, M., El Haddad, I., Eleftheriadis, K., Favez, O., Flentje, H., Font, A., Fossum, K., Freney, E., Gini, M., Green, D. C., Heikkinen, L., Herrmann, H., Kalogridis, A.-C., Keernik, H., Lhotka, R., Lin, C., Lunder, C., Maasikmets, M., Manousakas, M. I., Marchand, N., Marin, C., Marmureanu, L., Mihalopoulos, N., Moènik, G., Nêcki, J., O'Dowd, C., Ovadnevaite, J., Peter, T., Petit, J.-E., Pikridas, M., Matthew Platt, S., Pokorná, P., Poulain, L., Priestman, M., Riffault, V., Rinaldi, M., Ró¿añski, K., Schwarz, J., Sciare, J., Simon, L., Skiba, A., Slowik, J. G., Sosedova, Y., Stavroulas, I., Styszko, K., Teinemaa, E., Timonen, H., Tremper, A., Vasilescu, J., Via, M., Vodièka, P., Wiedensohler, A., Zografou, O., Cruz Minguillón, M., and Prévôt, A. S. H.: European aerosol phenomenology – 8: Harmonised source apportionment of organic aerosol using 22 Year-long ACSM/AMS datasets, Environ. Int., 166, 107325, https://doi.org/10.1016/j.envint.2022.107325, 2022.

Chen, J., Li, C., Ristovski, Z., Milic, A., Gu, Y., Islam, M. S., Wang, S., Hao, J., Zhang, H., He, C., Guo, H., Fu, H., Miljevic, B., Morawska, L., Thai, P., Lam, Y. F., Pereira, G., Ding, A., Huang, X., and Dumka, U. C.: A review of biomass burning: Emissions and impacts on air quality, health and climate in China, Sci. Total Environ., 579, 1000–1034, https://doi.org/10.1016/j.scitotenv.2016.11.025, 2017.

Chen, K., Mayorga, R., Raeofy, N., Lum, M., Woods, M., Bahreini, R., Zhang, H., and Lin, Y.-H.: Effects of Nitrate Radical Levels and Pre-Existing Particles on Secondary Brown Carbon Formation from Nighttime Oxidation of Furan, ACS Earth and Space Chemistry, 6, 2709–2721, https://doi.org/10.1021/acsearthspacechem.2c00244, 2022.

Cheng, Z., Atwi, K. M., Yu, Z., Avery, A., Fortner, E. C., Williams, L., Majluf, F., Krechmer, J. E., Lambe, A. T., and Saleh, R.: Evolution of the light-absorption properties of combustion brown carbon aerosols following reaction with nitrate radicals, Aerosol Sci. Technol., 54, 849–863, https://doi.org/10.1080/02786826.2020.1726867, 2020.

Crenn, V., Sciare, J., Croteau, P. L., Verlhac, S., Fröhlich, R., Belis, C. A., Aas, W., Äijälä, M., Alastuey, A., Artiñano, B., Baisnée, D., Bonnaire, N., Bressi, M., Canagaratna, M., Canonaco, F., Carbone, C., Cavalli, F., Coz, E., Cubison, M. J., Esser-Gietl, J. K., Green, D. C., Gros, V., Heikkinen, L., Herrmann, H., Lunder, C., Minguillón, M. C., Močnik, G., O'Dowd, C. D., Ovadnevaite, J., Petit, J.-E., Petralia, E., Poulain, L., Priestman, M., Riffault, V., Ripoll, A., Sarda-Estève, R., Slowik, J. G., Setyan, A., Wiedensohler, A., Baltensperger, U., Prévôt, A. S. H., Jayne, J. T., and Favez, O.: ACTRIS ACSM intercomparison – Part 1: Reproducibility of concentration and fragment results from 13 individual Quadrupole Aerosol Chemical Speciation Monitors (Q-ACSM) and consistency with co-located instruments, Atmos. Meas. Tech., 8, 5063–5087, https://doi.org/10.5194/amt-8-5063-2015, 2015.

Crippa, M., DeCarlo, P. F., Slowik, J. G., Mohr, C., Heringa, M. F., Chirico, R., Poulain, L., Freutel, F., Sciare, J., Cozic, J., Di Marco, C. F., Elsasser, M., Nicolas, J. B., Marchand, N., Abidi, E., Wiedensohler, A., Drewnick, F., Schneider, J., Borrmann, S., Nemitz, E., Zimmermann, R., Jaffrezo, J.-L., Prévôt, A. S. H., and Baltensperger, U.: Wintertime aerosol chemical composition and source apportionment of the organic fraction in the metropolitan area of Paris, Atmos. Chem. Phys., 13, 961–981, https://doi.org/10.5194/acp-13-961-2013, 2013.

Davis, D. D., Ravishankara, A. R., and Fischer, S.: SO_2 oxidation via the hydroxyl radical: Atmospheric fate of HSO_x radicals, Geophys. Res. Lett., 6, 113–116, https://doi.org/10.1029/GL006i002p00113, 1979.

DeCarlo, P. F., Slowik, J. G., Worsnop, D. R., Davidovits, P., and Jimenez, J. L.: Particle Morphology and Density Characterization by Combined Mobility and Aerodynamic Diameter Measurements. Part 1: Theory, Aerosol Sci. Technol., 38, 1185–1205, https://doi.org/10.1080/027868290903907, 2004.

Denier van der Gon, H. A. C., Bergström, R., Fountoukis, C., Johansson, C., Pandis, S. N., Simpson, D., and Visschedijk, A. J. H.: Particulate emissions from residential wood combustion in Europe – revised estimates and an evaluation, Atmos. Chem. Phys., 15, 6503–6519, https://doi.org/10.5194/acp-15-6503-2015, 2015.

Dingle, J. H., Zimmerman, S., Frie, A. L., Min, J., Jung, H., and Bahreini, R.: Complex refractive index, single scattering albedo, and mass absorption coefficient of secondary organic aerosols generated from oxidation of biogenic and anthropogenic precursors, Aerosol Sci. Technol., 53, 449–463, https://doi.org/10.1080/02786826.2019.1571680, 2019.

Drinovec, L., Močnik, G., Zotter, P., Prévôt, A. S. H., Ruckstuhl, C., Coz, E., Rupakheti, M., Sciare, J., Müller, T., Wiedensohler, A., and Hansen, A. D. A.: The "dual-spot" Aethalometer: an improved measurement of aerosol black carbon with real-time loading compensation, Atmos. Meas. Tech., 8, 1965–1979, https://doi.org/10.5194/amt-8-1965-2015, 2015.

Drinovec, L., Gregorič, A., Zotter, P., Wolf, R., Bruns, E. A., Prévôt, A. S. H., Petit, J.-E., Favez, O., Sciare, J., Arnold, I. J., Chakrabarty, R. K., Moosmüller, H., Filep, A., and Močnik, G.: The filter-loading effect by ambient aerosols in filter absorption photometers depends on the coating of the sampled particles, Atmos. Meas. Tech., 10, 1043–1059, https://doi.org/10.5194/amt-10-1043-2017, 2017.

Drinovec, L., Jagodič, U., Pirker, L., Škarabot, M., Kurtjak, M., Vidović, K., Ferrero, L., Visser, B., Röhrbein, J., Weingartner, E., Kalbermatter, D. M., Vasilatou, K., Bühlmann, T., Pascale, C., Müller, T., Wiedensohler, A., and Močnik, G.: A dual-wavelength photothermal aerosol absorption monitor: design, calibration and performance, Atmos. Meas. Tech., 15, 3805–3825, https://doi.org/10.5194/amt-15-3805-2022, 2022.

El Mais, A. E. R.: Primary and secondary residential wood combustion emissions: physicochemical and bio-analytical characterization and effect-directed analysis (EDA), PhD Thesis, Université Aix Marseille, 2023.

Finlayson-Pitts, B. J. and Pitts, J. N.: Chemistry of the upper and lower atmosphere: theory, experiments, and applications, Nachdr., Academic Press, San Diego, Calif., 969 pp., https://doi.org/10.1016/B978-0-12-257060-5.X5000-X, 2000.

Fountoukis, C., Megaritis, A. G., Skyllakou, K., Charalampidis, P. E., Denier van der Gon, H. A. C., Crippa, M., Prévôt, A. S. H., Fachinger, F., Wiedensohler, A., Pilinis, C., and Pandis, S. N.: Simulating the formation of carbonaceous aerosol in a European Megacity (Paris) during the MEGAPOLI summer and winter campaigns, Atmos. Chem. Phys., 16, 3727–3741, https://doi.org/10.5194/acp-16-3727-2016, 2016.

Freney, E., Zhang, Y., Croteau, P., Amodeo, T., Williams, L., Truong, F., Petit, J.-E., Sciare, J., Sarda-Esteve, R., Bonnaire, N., Arumae, T., Aurela, M., Bougiatioti, A., Mihalopoulos, N., Coz, E., Artinano, B., Crenn, V., Elste, T., Heikkinen, L., Poulain, L., Wiedensohler, A., Herrmann, H., Priestman, M., Alastuey, A., Stavroulas, I., Tobler, A., Vasilescu, J., Zanca, N., Canagaratna, M., Carbone, C., Flentje, H., Green, D., Maasikmets, M., Marmureanu, L., Minguillon, M. C., Prevot, A. S. H., Gros, V., Jayne, J., and Favez, O.: The second ACTRIS inter-comparison (2016) for Aerosol Chemical Speciation Monitors (ACSM): Calibration protocols and instrument performance evaluations, Aerosol Sci. Technol., 53, 830–842, https://doi.org/10.1080/02786826.2019.1608901, 2019.

Fuzzi, S., Baltensperger, U., Carslaw, K., Decesari, S., Denier van der Gon, H., Facchini, M. C., Fowler, D., Koren, I., Langford, B., Lohmann, U., Nemitz, E., Pandis, S., Riipinen, I., Rudich, Y., Schaap, M., Slowik, J. G., Spracklen, D. V., Vignati, E., Wild, M., Williams, M., and Gilardoni, S.: Particulate matter, air quality and climate: lessons learned and future needs, Atmos. Chem. Phys., 15, 8217–8299, https://doi.org/10.5194/acp-15-8217-2015, 2015.

Gómez Alvarez, E., Borrás, E., Viidanoja, J., and Hjorth, J.: Unsaturated dicarbonyl products from the OH-initiated photo-oxidation of furan, 2-methylfuran and 3-methylfuran, Atmos. Environ., 43, 1603–1612, https://doi.org/10.1016/j.atmosenv.2008.12.019, 2009.

Hallquist, M., Wenger, J. C., Baltensperger, U., Rudich, Y., Simpson, D., Claeys, M., Dommen, J., Donahue, N. M., George, C., Goldstein, A. H., Hamilton, J. F., Herrmann, H., Hoffmann, T., Iinuma, Y., Jang, M., Jenkin, M. E., Jimenez, J. L., Kiendler-Scharr, A., Maenhaut, W., McFiggans, G., Mentel, Th. F., Monod, A., Prévôt, A. S. H., Seinfeld, J. H., Surratt, J. D.,

Szmigielski, R., and Wildt, J.: The formation, properties and impact of secondary organic aerosol: current and emerging issues, Atmos. Chem. Phys., 9, 5155–5236, https://doi.org/10.5194/acp-9-5155-2009, 2009.

Hartikainen, A., Yli-Pirilä, P., Tiitta, P., Leskinen, A., Kortelainen, M., Orasche, J., Schnelle-Kreis, J., Lehtinen, K. E. J., Zimmermann, R., Jokiniemi, J., and Sippula, O.: Volatile Organic Compounds from Logwood Combustion: Emissions and Transformation under Dark and Photochemical Aging Conditions in a Smog Chamber, Environ. Sci. Technol., 52, 4979–4988, https://doi.org/10.1021/acs.est.7b06269, 2018.

Hatch, L. E., Luo, W., Pankow, J. F., Yokelson, R. J., Stockwell, C. E., and Barsanti, K. C.: Identification and quantification of gaseous organic compounds emitted from biomass burning using two-dimensional gas chromatography–time-of-flight mass spectrometry, Atmos. Chem. Phys., 15, 1865–1899, https://doi.org/10.5194/acp-15-1865-2015, 2015.

Hatch, L. E., Yokelson, R. J., Stockwell, C. E., Veres, P. R., Simpson, I. J., Blake, D. R., Orlando, J. J., and Barsanti, K. C.: Multi-instrument comparison and compilation of non-methane organic gas emissions from biomass burning and implications for smoke-derived secondary organic aerosol precursors, Atmos. Chem. Phys., 17, 1471–1489, https://doi.org/10.5194/acp-17-1471-2017, 2017.

Hatch, L. E., Rivas-Ubach, A., Jen, C. N., Lipton, M., Goldstein, A. H., and Barsanti, K. C.: Measurements of I/SVOCs in biomass-burning smoke using solid-phase extraction disks and two-dimensional gas chromatography, Atmos. Chem. Phys., 18, 17801–17817, https://doi.org/10.5194/acp-18-17801-2018, 2018.

He, Q., Li, C., Siemens, K., Morales, A. C., Hettiyadura, A. P. S., Laskin, A., and Rudich, Y.: Optical Properties of Secondary Organic Aerosol Produced by Photooxidation of Naphthalene under NO_x Condition, Environ. Sci. Technol., 56, 4816–4827, https://doi.org/10.1021/acs.est.1c07328, 2022.

Heald, C. L. and Kroll, J. H.: The fuel of atmospheric chemistry: Toward a complete description of reactive organic carbon, Sci. Adv., 6, eaay8967, https://doi.org/10.1126/sciadv.aay8967, 2020.

Hems, R. F., Schnitzler, E. G., Liu-Kang, C., Cappa, C. D., and Abbatt, J. P. D.: Aging of Atmospheric Brown Carbon Aerosol, ACS Earth Space Chem., 5, 722–748, https://doi.org/10.1021/acsearthspacechem.0c00346, 2021.

Hodshire, A. L., Akherati, A., Alvarado, M. J., Brown-Steiner, B., Jathar, S. H., Jimenez, J. L., Kreidenweis, S. M., Lonsdale, C. R., Onasch, T. B., Ortega, A. M., and Pierce, J. R.: Aging Effects on Biomass Burning Aerosol Mass and Composition: A Critical Review of Field and Laboratory Studies, Environ. Sci. Technol., 53, 10007–10022, https://doi.org/10.1021/acs.est.9b02588, 2019.

Hoffer, A., Gelencsér, A., Guyon, P., Kiss, G., Schmid, O., Frank, G. P., Artaxo, P., and Andreae, M. O.: Optical properties of humic-like substances (HULIS) in biomass-burning aerosols, Atmos. Chem. Phys., 6, 3563–3570, https://doi.org/10.5194/acp-6-3563-2006, 2006.

Iaukea-Lum, M., Bhattarai, C., Sengupta, D., Samburova, V., Khlystov, A. Y., Watts, A. C., Arnott, W. P., and Moosmüller, H.: Optical Characterization of Fresh and Photochemically Aged Aerosols Emitted from Laboratory Siberian Peat Burning, Atmosphere, 13, 386, https://doi.org/10.3390/atmos13030386, 2022.

IPCC: Climate Change 2022: Impacts, Adaptation and Vulnerability. Contribution of Working Group II to the Sixth Assessment Report of the Intergovernmental Panel on Climate Change, edited by: Pörtner, H.-O., Roberts, D. C., Tignor, M. M. B., Poloczanska, E. S., Mintenbeck, K., Alegría, A., Craig, M., Langsdorf, S., Löschke, S., Möller, V., Okem, A., and Rama, B., Cambridge University Press, Cambridge, UK and New York, NY, USA, https://doi.org/10.1017/9781009325844, 2022.

Jiang, H., Frie, A. L., Lavi, A., Chen, J. Y., Zhang, H., Bahreini, R., and Lin, Y.-H.: Brown Carbon Formation from Nighttime Chemistry of Unsaturated Heterocyclic Volatile Organic Compounds, Environ. Sci. Technol. Lett., 6, 184–190, https://doi.org/10.1021/acs.estlett.9b00017, 2019.

Jiang, J., Carter, W. P. L., Cocker, D. R. I., and Barsanti, K. C.: Development and Evaluation of a Detailed Mechanism for Gas-Phase Atmospheric Reactions of Furans, ACS Earth Space Chem., 4, 1254–1268, https://doi.org/10.1021/acsearthspacechem.0c00058, 2020.

Jiang, X., Tsona, N. T., Jia, L., Liu, S., Zhang, H., Xu, Y., and Du, L.: Secondary organic aerosol formation from photooxidation of furan: effects of NOx and humidity, Atmos. Chem. Phys., 19, 13591–13609, https://doi.org/10.5194/acp-19-13591-2019, 2019.

Jimenez, J. L., Canagaratna, M. R., Donahue, N. M., Prevot, A. S. H., Zhang, Q., Kroll, J. H., DeCarlo, P. F., Allan, J. D., Coe, H., Ng, N. L., Aiken, A. C., Docherty, K. S., Ulbrich, I. M., Grieshop, A. P., Robinson, A. L., Duplissy, J., Smith, J. D., Wilson, K. R., Lanz, V. A., Hueglin, C., Sun, Y. L., Tian, J., Laaksonen, A., Raatikainen, T., Rautiainen, J., Vaattovaara, P., Ehn, M., Kulmala, M., Tomlinson, J. M., Collins, D. R., Cubison, M. J., E., Dunlea, J., Huffman, J. A., Onasch, T. B., Alfarra, M. R., Williams, P. I., Bower, K., Kondo, Y., Schneider, J., Drewnick, F., Borrmann, S., Weimer, S., Demerjian, K., Salcedo, D., Cottrell, L., Griffin, R., Takami, A., Miyoshi, T., Hatakeyama, S., Shimono, A., Sun, J. Y., Zhang, Y. M., Dzepina, K., Kimmel, J. R., Sueper, D., Jayne, J. T., Herndon, S. C., Trimborn, A. M., Williams, L. R., Wood, E. C., Middlebrook, A. M., Kolb, C. E., Baltensperger, U., and Worsnop, D. R.: Evolution of Organic Aerosols in the Atmosphere, Science, 326, 1525–1529, https://doi.org/10.1126/science.1180353, 2009.

Johnson, T. J., Symonds, J. P. R., and Olfert, J. S.: Mass–Mobility Measurements Using a Centrifugal Particle Mass Analyzer and Differential Mobility Spectrometer, Aerosol Sci. Technol., 47, 1215–1225, https://doi.org/10.1080/02786826.2013.830692, 2013.

Joo, T., Rivera-Rios, J. C., Takeuchi, M., Alvarado, M. J., and Ng, N. L.: Secondary Organic Aerosol Formation from Reaction of 3-Methylfuran with Nitrate Radicals, ACS Earth Space Chem., 3, 922–934, https://doi.org/10.1021/acsearthspacechem.9b00068, 2019.

Jorga, S. D., Florou, K., Kaltsonoudis, C., Kodros, J. K., Vasilakopoulou, C., Cirtog, M., Fouqueau, A., Picquet-Varrault, B., Nenes, A., and Pandis, S. N.: Nighttime chemistry of biomass burning emissions in urban areas: A dual mobile chamber study, Atmos. Chem. Phys., 21, 15337–15349, https://doi.org/10.5194/acp-21-15337-2021, 2021.

Kang, E., Root, M. J., Toohey, D. W., and Brune, W. H.: Introducing the concept of Potential Aerosol Mass (PAM), Atmos. Chem.

Phys., 7, 5727–5744, https://doi.org/10.5194/acp-7-5727-2007, 2007.

Kautzman, K. E., Surratt, J. D., Chan, M. N., Chan, A. W. H., Hersey, S. P., Chhabra, P. S., Dalleska, N. F., Wennberg, P. O., Flagan, R. C., and Seinfeld, J. H.: Chemical Composition of Gas- and Aerosol-Phase Products from the Photooxidation of Naphthalene, J. Phys. Chem. A, 114, 913–934, https://doi.org/10.1021/jp908530s, 2010.

Keyte, I. J., Harrison, R. M., and Lammel, G.: Chemical reactivity and long-range transport potential of polycyclic aromatic hydrocarbons – a review, Chem. Soc. Rev., 42, 9333, https://doi.org/10.1039/c3cs60147a, 2013.

Khan, F., Kwapiszewska, K., Zhang, Y., Chen, Y., Lambe, A. T., Kołodziejczyk, A., Jalal, N., Rudzinski, K., Martínez-Romero, A., Fry, R. C., Surratt, J. D., and Szmigielski, R.: Toxicological Responses of á-Pinene-Derived Secondary Organic Aerosol and Its Molecular Tracers in Human Lung Cell Lines, Chem. Res. Toxicol., 34, 817–832, https://doi.org/10.1021/acs.chemrestox.0c00409, 2021.

Kind, I., Berndt, T., Böge, O., and Rolle, W.: Gas-phase rate constants for the reaction of NO_3 radicals with furan and methyl-substituted furans, Chem. Phys. Lett., 256, 679–683, 1996.

Kleindienst, T. E., Jaoui, M., Lewandowski, M., Offenberg, J. H., and Docherty, K. S.: The formation of SOA and chemical tracer compounds from the photooxidation of naphthalene and its methyl analogs in the presence and absence of nitrogen oxides, Atmos. Chem. Phys., 12, 8711–8726, https://doi.org/10.5194/acp-12-8711-2012, 2012.

Klodt, A., Aiona, P., MacMillan, A., Lee, H. J. (Julie), Zhang, X., Helgestad, T., Novak, G., Lin, P., Laskin, J., Laskin, A., Bertram, T., Cappa, C., and Nizkorodov, S. A.: Effect of Relative Humidity, NOx, and Ammonia on Physical Properties of Naphthalene Secondary Organic Aerosol, Environ. Sci.-Atmos., 3, 991–1007, https://doi.org/10.1039/D3EA00033H, 2023.

Kodros, J. K., Papanastasiou, D. K., Paglione, M., Masiol, M., Squizzato, S., Florou, K., Skyllakou, K., Kaltsonoudis, C., Nenes, A., and Pandis, S. N.: Rapid dark aging of biomass burning as an overlooked source of oxidized organic aerosol, P. Natl. Acad. Sci. USA, 117, 33028–33039, 2020.

Kodros, J. K., Kaltsonoudis, C., Paglione, M., Florou, K., Jorga, S., Vasilakopoulou, C., Cirtog, M., Cazaunau, M., Picquet-Varrault, B., Nenes, A., and Pandis, S. N.: Secondary aerosol formation during the dark oxidation of residential biomass burning emissions, Environ. Sci.-Atmos., 2, 1221–1236, https://doi.org/10.1039/D2EA00031H, 2022.

Kostenidou, E., Pathak, R. K., and Pandis, S. N.: An Algorithm for the Calculation of Secondary Organic Aerosol Density Combining AMS and SMPS Data, Aerosol Sci. Technol., 41, 1002–1010, https://doi.org/10.1080/02786820701666270, 2007.

Kroll, J. H. and Seinfeld, J. H.: Chemistry of secondary organic aerosol: Formation and evolution of low-volatility organics in the atmosphere, Atmos. Environ., 42, 3593–3624, https://doi.org/10.1016/j.atmosenv.2008.01.003, 2008.

Kwamena, N.-O. A. and Abbatt, J. P. D.: Heterogeneous nitration reactions of polycyclic aromatic hydrocarbons and n-hexane soot by exposure to $NO_3/NO_2/N_2O_5$, Atmos. Environ., 42, 8309–8314, https://doi.org/10.1016/j.atmosenv.2008.07.037, 2008.

Lack, D. A., Langridge, J. M., Bahreini, R., Cappa, C. D., Middlebrook, A. M., and Schwarz, J. P.: Brown carbon and internal mixing in biomass burning particles, P. Natl. Acad. Sci. USA, 109, 14802–14807, https://doi.org/10.1073/pnas.1206575109, 2012.

Lambe, A. T., Ahern, A. T., Williams, L. R., Slowik, J. G., Wong, J. P. S., Abbatt, J. P. D., Brune, W. H., Ng, N. L., Wright, J. P., Croasdale, D. R., Worsnop, D. R., Davidovits, P., and Onasch, T. B.: Characterization of aerosol photooxidation flow reactors: heterogeneous oxidation, secondary organic aerosol formation and cloud condensation nuclei activity measurements, Atmos. Meas. Tech., 4, 445–461, https://doi.org/10.5194/amt-4-445-2011, 2011.

Lambe, A. T., Cappa, C. D., Massoli, P., Onasch, T. B., Forestieri, S. D., Martin, A. T., Cummings, M. J., Croasdale, D. R., Brune, W. H., Worsnop, D. R., and Davidovits, P.: Relationship between Oxidation Level and Optical Properties of Secondary Organic Aerosol, Environ. Sci. Technol., 47, 6349–6357, https://doi.org/10.1021/es401043j, 2013.

Lambe, A. T., Chhabra, P. S., Onasch, T. B., Brune, W. H., Hunter, J. F., Kroll, J. H., Cummings, M. J., Brogan, J. F., Parmar, Y., Worsnop, D. R., Kolb, C. E., and Davidovits, P.: Effect of oxidant concentration, exposure time, and seed particles on secondary organic aerosol chemical composition and yield, Atmos. Chem. Phys., 15, 3063–3075, https://doi.org/10.5194/acp-15-3063-2015, 2015.

Lambe, A. T., Wood, E. C., Krechmer, J. E., Majluf, F., Williams, L. R., Croteau, P. L., Cirtog, M., Féron, A., Petit, J.-E., Albinet, A., Jimenez, J. L., and Peng, Z.: Nitrate radical generation via continuous generation of dinitrogen pentoxide in a laminar flow reactor coupled to an oxidation flow reactor, Atmos. Meas. Tech., 13, 2397–2411, https://doi.org/10.5194/amt-13-2397-2020, 2020.

Laskin, A., Laskin, J., and Nizkorodov, S. A.: Chemistry of Atmospheric Brown Carbon, Chem. Rev., 115, 4335–4382, https://doi.org/10.1021/cr5006167, 2015.

Lau, Y.-S., Chan, M.-N., Poon, H.-Y., Tan, Y., Lee, S.-C., Li, J., and Ho, K.-F.: Chemical Composition of Gas and Particle Phase Products of Toluene Photooxidation Reaction under High OH Exposure Condition, Atmosphere, 12, 915, https://doi.org/10.3390/atmos12070915, 2021.

Lee, H. J. (Julie), Aiona, P. K., Laskin, A., Laskin, J., and Nizkorodov, S. A.: Effect of Solar Radiation on the Optical Properties and Molecular Composition of Laboratory Proxies of Atmospheric Brown Carbon, Environ. Sci. Technol., 48, 10217–10226, https://doi.org/10.1021/es502515r, 2014.

Lee, J. and Lane, D. A.: Formation of oxidized products from the reaction of gaseous phenanthrene with the OH radical in a reaction chamber, Atmos. Environ., 44, 2469–2477, https://doi.org/10.1016/j.atmosenv.2010.03.008, 2010.

Lee, J. Y. and Lane, D. A.: Unique products from the reaction of naphthalene with the hydroxyl radical, Atmos. Environ., 43, 4886–4893, https://doi.org/10.1016/j.atmosenv.2009.07.018, 2009.

Lee, J. Y., Lane, D. A., Heo, J. B., Yi, S.-M., and Kim, Y. P.: Quantification and seasonal pattern of atmospheric reaction products of gas phase PAHs in $PM_{2.5}$, Atmos. Environ., 55, 17–25, https://doi.org/10.1016/j.atmosenv.2012.03.007, 2012.

Li, M., Liu, Y., and Wang, L.: Gas-phase ozonolysis of furans, methylfurans, and dimethylfurans in the atmosphere, Phys. Chem. Chem. Phys., 20, 24735–24743, https://doi.org/10.1039/C8CP04947E, 2018.

Li, R., Palm, B. B., Ortega, A. M., Hlywiak, J., Hu, W., Peng, Z., Day, D. A., Knote, C., Brune, W. H., de Gouw, J. A., and Jimenez, J. L.: Modeling the Radical Chemistry in an Oxidation Flow Reactor: Radical Formation and Recycling, Sensitivities, and the OH Exposure Estimation Equation, J. Phys. Chem. A, 119, 4418–4432, https://doi.org/10.1021/jp509534k, 2015.

Liu, J., Lin, P., Laskin, A., Laskin, J., Kathmann, S. M., Wise, M., Caylor, R., Imholt, F., Selimovic, V., and Shilling, J. E.: Optical properties and aging of light-absorbing secondary organic aerosol, Atmos. Chem. Phys., 16, 12815–12827, https://doi.org/10.5194/acp-16-12815-2016, 2016.

Liu, P. F., Abdelmalki, N., Hung, H.-M., Wang, Y., Brune, W. H., and Martin, S. T.: Ultraviolet and visible complex refractive indices of secondary organic material produced by photooxidation of the aromatic compounds toluene and *m*-xylene, Atmos. Chem. Phys., 15, 1435–1446, https://doi.org/10.5194/acp-15-1435-2015, 2015.

Liu, Y. and Daum, P. H.: Relationship of refractive index to mass density and self-consistency of mixing rules for multicomponent mixtures like ambient aerosols, J. Aerosol Sci., 39, 974–986, https://doi.org/10.1016/j.jaerosci.2008.06.006, 2008.

Lu, J. W., Flores, J. M., Lavi, A., Abo-Riziq, A., and Rudich, Y.: Changes in the optical properties of benzo[a]pyrene-coated aerosols upon heterogeneous reactions with NO_2 and NO_3, Phys. Chem. Chem. Phys., 13, 6484–6492, https://doi.org/10.1039/C0CP02114H, 2011.

Malloy, Q. G. J., Nakao, S., Qi, L., Austin, R., Stothers, C., Hagino, H., and Cocker, D. R.: Real-Time Aerosol Density Determination Utilizing a Modified Scanning Mobility Particle Sizer – Aerosol Particle Mass Analyzer System, Aerosol Sci. Technol., 43, 673–678, https://doi.org/10.1080/02786820902832960, 2009.

Mao, J., Ren, X., Brune, W. H., Olson, J. R., Crawford, J. H., Fried, A., Huey, L. G., Cohen, R. C., Heikes, B., Singh, H. B., Blake, D. R., Sachse, G. W., Diskin, G. S., Hall, S. R., and Shetter, R. E.: Airborne measurement of OH reactivity during INTEX-B, Atmos. Chem. Phys., 9, 163–173, https://doi.org/10.5194/acp-9-163-2009, 2009.

Mbengue, S., Zikova, N., Schwarz, J., Vodièka, P., Šmejkalová, A. H., and Holoubek, I.: Mass absorption cross-section and absorption enhancement from long term black and elemental carbon measurements: A rural background station in Central Europe, Sci. Total Environ., 794, 148365, https://doi.org/10.1016/j.scitotenv.2021.148365, 2021.

McMurry, P. H., Wang, X., Park, K., and Ehara, K.: The Relationship between Mass and Mobility for Atmospheric Particles: A New Technique for Measuring Particle Density, Aerosol Sci. Technol., 36, 227–238, https://doi.org/10.1080/027868202753504083, 2002.

Metcalf, A. R., Loza, C. L., Coggon, M. M., Craven, J. S., Jonsson, H. H., Flagan, R. C., and Seinfeld, J. H.: Secondary Organic Aerosol Coating Formation and Evaporation: Chamber Studies Using Black Carbon Seed Aerosol and the Single-Particle Soot Photometer, Aerosol Sci. Technol., 47, 326–347, https://doi.org/10.1080/02786826.2012.750712, 2013.

Mircea, M., Bessagnet, B., D'Isidoro, M., Pirovano, G., Aksoyoglu, S., Ciarelli, G., Tsyro, S., Manders, A., Bieser, J., Stern, R., Vivanco, M. G., Cuvelier, C., Aas, W., Prévôt, A. S. H., Aulinger, A., Briganti, G., Calori, G., Cappelletti, A., Colette, A., Couvidat, F., Fagerli, H., Finardi, S., Kranenburg, R., Rouïl, L., Silibello, C., Spindler, G., Poulain, L., Herrmann, H., Jimenez, J. L., Day, D. A., Tiitta, P., and Carbone, S.: EURODELTA III exercise: An evaluation of air quality models' capacity to reproduce the carbonaceous aerosol, Atmos. Environ. X, 2, 100018, https://doi.org/10.1016/j.aeaoa.2019.100018, 2019.

Moise, T., Flores, J. M., and Rudich, Y.: Optical Properties of Secondary Organic Aerosols and Their Changes by Chemical Processes, Chem. Rev., 115, 4400–4439, https://doi.org/10.1021/cr5005259, 2015.

Monks, P. S., Granier, C., Fuzzi, S., Stohl, A., Williams, M. L., Akimoto, H., Amann, M., Baklanov, A., Baltensperger, U., Bey, I., Blake, N., Blake, R. S., Carslaw, K., Cooper, O. R., Dentener, F., Fowler, D., Fragkou, E., Frost, G. J., Generoso, S., Ginoux, P., Grewe, V., Guenther, A., Hansson, H. C., Henne, S., Hjorth, J., Hofzumahaus, A., Huntrieser, H., Isaksen, I. S. A., Jenkin, M. E., Kaiser, J., Kanakidou, M., Klimont, Z., Kulmala, M., Laj, P., Lawrence, M. G., Lee, J. D., Liousse, C., Maione, M., McFiggans, G., Metzger, A., Mieville, A., Moussiopoulos, N., Orlando, J. J., O'Dowd, C. D., Palmer, P. I., Parrish, D. D., Petzold, A., Platt, U., Pöschl, U., Prévôt, A. S. H., Reeves, C. E., Reimann, S., Rudich, Y., Sellegri, K., Steinbrecher, R., Simpson, D., ten Brink, H., Theloke, J., van der Werf, G. R., Vautard, R., Vestreng, V., Vlachokostas, Ch., and von Glasow, R.: Atmospheric composition change – global and regional air quality, Atmos. Environ., 43, 5268–5350, https://doi.org/10.1016/j.atmosenv.2009.08.021, 2009.

Nakao, S., Tang, P., Tang, X., Clark, C. H., Qi, L., Seo, E., Asa-Awuku, A., and Cocker, D.: Density and elemental ratios of secondary organic aerosol: Application of a density prediction method, Atmos. Environ., 68, 273–277, https://doi.org/10.1016/j.atmosenv.2012.11.006, 2013.

Nalin, F., Golly, B., Besombes, J.-L., Pelletier, C., Aujay-Plouzeau, R., Verlhac, S., Dermigny, A., Fievet, A., Karoski, N., Dubois, P., Collet, S., Favez, O., and Albinet, A.: Fast oxidation processes from emission to ambient air introduction of aerosol emitted by residential log wood stoves, Atmos. Environ., 143, 15–26, https://doi.org/10.1016/j.atmosenv.2016.08.002, 2016.

Newland, M. J., Ren, Y., McGillen, M. R., Michelat, L., Daële, V., and Mellouki, A.: NO3 chemistry of wildfire emissions: a kinetic study of the gas-phase reactions of furans with the NO_3 radical, Atmos. Chem. Phys., 22, 1761–1772, https://doi.org/10.5194/acp-22-1761-2022, 2022.

Ng, N. L., Herndon, S. C., Trimborn, A., Canagaratna, M. R., Croteau, P. L., Onasch, T. B., Sueper, D., Worsnop, D. R., Zhang, Q., Sun, Y. L., and Jayne, J. T.: An Aerosol Chemical Speciation Monitor (ACSM) for Routine Monitoring of the Composition and Mass Concentrations of Ambient Aerosol, Aerosol Sci. Technol., 45, 780–794, https://doi.org/10.1080/02786826.2011.560211, 2011.

Offer, S., Hartner, E., Di, B. S., Bisig, C., Bauer, S., Pantzke, J., Zimmermann, E. J., Cao, X., Binder, S., Kuhn, E., Huber, A., Jeong, S., K, äfer U., Martens, P., Mesceriakovas, A., Bendl, J., Brejcha, R., Buchholz, A., Gat, D., Hohaus, T., Rastak, N., Jakobi, G., Kalberer, M., Kanashova, T., Hu, Y., Ogris, C., Marsico, A., Theis, F., Pardo, M., Gr, öger T., Oeder, S., Orasche, J., Paul, A., Ziehm, T., Zhang, Z.-H., Adam, T., Sippula, O., Sklorz, M., Schnelle, -Kreis Jürgen, Czech, H., Kiendler, -Scharr Astrid, Rudich, Y., and Zimmermann, R.: Effect of Atmospheric Aging on Soot Particle Toxicity in Lung Cell Models at the Air–Liquid

Interface: Differential Toxicological Impacts of Biogenic and Anthropogenic Secondary Organic Aerosols (SOAs), Environ. Health Persp., 130, 027003, https://doi.org/10.1289/EHP9413, 2022.

Olfert, J. S. and Collings, N.: New method for particle mass classification – the Couette centrifugal particle mass analyzer, J. Aerosol Sci., 36, 1338–1352, https://doi.org/10.1016/j.jaerosci.2005.03.006, 2005.

Olfert, J. S., Reavell, K. StJ., Rushton, M. G., and Collings, N.: The experimental transfer function of the Couette centrifugal particle mass analyzer, J. Aerosol Sci., 37, 1840–1852, https://doi.org/10.1016/j.jaerosci.2006.07.007, 2006.

Ortega, A. M., Day, D. A., Cubison, M. J., Brune, W. H., Bon, D., de Gouw, J. A., and Jimenez, J. L.: Secondary organic aerosol formation and primary organic aerosol oxidation from biomass-burning smoke in a flow reactor during FLAME-3, Atmos. Chem. Phys., 13, 11551–11571, https://doi.org/10.5194/acp-13-11551-2013, 2013.

Peng, L., Li, Z., Zhang, G., Bi, X., Hu, W., Tang, M., Wang, X., Peng, P., and Sheng, G.: A review of measurement techniques for aerosol effective density, Sci. Total Environ., 778, 146248, https://doi.org/10.1016/j.scitotenv.2021.146248, 2021.

Peng, Z. and Jimenez, J. L.: KinSim: A Research-Grade, User-Friendly, Visual Kinetics Simulator for Chemical-Kinetics and Environmental-Chemistry Teaching, J. Chem. Educ., 96, 806–811, https://doi.org/10.1021/acs.jchemed.9b00033, 2019.

Peng, Z. and Jimenez, J. L.: Radical chemistry in oxidation flow reactors for atmospheric chemistry research, Chem. Soc. Rev., 49, 2570–2616, https://doi.org/10.1039/C9CS00766K, 2020.

Pope, C. A., Burnett, R. T., Thun, M. J., Calle, E. E., Krewski, D., Ito, K., and Thurston, G. D.: Lung Cancer, Cardiopulmonary Mortality, and Long-term Exposure to Fine Particulate Air Pollution, JAMA, 287, 1132–1141, https://doi.org/10.1001/jama.287.9.1132, 2002.

Pope, C. A., Coleman, N., Pond, Z. A., and Burnett, R. T.: Fine particulate air pollution and human mortality: 25+ years of cohort studies, Environ. Res., 183, 108924, https://doi.org/10.1016/j.envres.2019.108924, 2020.

Rajagopalan, S., Al, -Kindi Sadeer G., and Brook, R. D.: Air Pollution and Cardiovascular Disease, J. Am. Coll. Cardiol., 72, 2054–2070, https://doi.org/10.1016/j.jacc.2018.07.099, 2018.

Reece, S. M., Sinha, A., and Grieshop, A. P.: Primary and Photochemically Aged Aerosol Emissions from Biomass Cookstoves: Chemical and Physical Characterization, Environ. Sci. Technol., 51, 9379–9390, https://doi.org/10.1021/acs.est.7b01881, 2017.

Reisen, F., Wheeler, S., and Arey, J.: Methyl- and dimethyl-/ethyl-nitronaphthalenes measured in ambient air in Southern California, Atmos. Environ., 37, https://doi.org/10.1016/S1352-2310(03)00469-2, 2003.

Ringuet, J., Albinet, A., Leoz-Garziandia, E., Budzinski, H., and Villenave, E.: Reactivity of polycyclic aromatic compounds (PAHs, NPAHs and OPAHs) adsorbed on natural aerosol particles exposed to atmospheric oxidants, Atmos. Environ., 61, 15–22, https://doi.org/10.1016/j.atmosenv.2012.07.025, 2012.

Riva, M., Healy, R. M., Flaud, P.-M., Perraudin, E., Wenger, J. C., and Villenave, E.: Gas- and particle-phase products from the photooxidation of acenaphthene and acenaphthylene by OH radicals, Atmos. Environ., 151, 34–44, https://doi.org/10.1016/j.atmosenv.2016.11.063, 2017.

Rùžièková, J., Raclavská, H., Juchelková, D., Kucbel, M., and Slamová, K.: The origin of potential precursors of secondary organic aerosols during combustion of biochar and softwood in residential heating, Process Saf. Environ., 161, 147–161, https://doi.org/10.1016/j.psep.2022.03.036, 2022.

Saleh, R., Marks, M., Heo, J., Adams, P. J., Donahue, N. M., and Robinson, A. L.: Contribution of brown carbon and lensing to the direct radiative effect of carbonaceous aerosols from biomass and biofuel burning emissions, J. Geophys. Res.-Atmos., 120, 10285–10296, https://doi.org/10.1002/2015JD023697, 2015.

Schauer, J. J., Kleeman, M. J., Cass, G. R., and Simoneit, B. R. T.: Measurement of Emissions from Air Pollution Sources. 3. C1-C29 Organic Compounds from Fireplace Combustion of Wood, Environ. Sci. Technol., 35, 1716–1728, https://doi.org/10.1021/es001331e, 2001.

Schervish, M. and Donahue, N. M.: Peroxy radical kinetics and new particle formation, Environ. Sci.-Atmos., 1, 79–92, https://doi.org/10.1039/D0EA00017E, 2021.

Seinfeld, J. H. and Pandis, S. N.: Atmospheric chemistry and physics: From air pollution to climate change, Wiley-Interscience, 1152 pp., ISBN 978-1-119-22117-3, 2016.

Shakya, K. M. and Griffin, R. J.: Secondary Organic Aerosol from Photooxidation of Polycyclic Aromatic Hydrocarbons, Environ. Sci. Technol., 44, 8134–8139, https://doi.org/10.1021/es1019417, 2010.

Siemens, K., Morales, A., He, Q., Li, C., Hettiyadura, A. P. S., Rudich, Y., and Laskin, A.: Molecular Analysis of Secondary Brown Carbon Produced from the Photooxidation of Naphthalene, Environ. Sci. Technol., 56, 3340–3353, https://doi.org/10.1021/acs.est.1c03135, 2022.

Soleimanian, E., Mousavi, A., Taghvaee, S., Shafer, M. M., and Sioutas, C.: Impact of secondary and primary particulate matter (PM) sources on the enhanced light absorption by brown carbon (BrC) particles in central Los Angeles, Sci. Total Environ., 705, 135902, https://doi.org/10.1016/j.scitotenv.2019.135902, 2020.

Srivastava, D., Favez, O., Perraudin, E., Villenave, E., and Albinet, A.: Comparison of Measurement-Based Methodologies to Apportion Secondary Organic Carbon (SOC) in $PM_{2.5}$: A Review of Recent Studies, Atmosphere, 9, 452, https://doi.org/10.3390/atmos9110452, 2018a.

Srivastava, D., Tomaz, S., Favez, O., Lanzafame, G. M., Golly, B., Besombes, J.-L., Alleman, L. Y., Jaffrezo, J.-L., Jacob, V., Perraudin, E., Villenave, E., and Albinet, A.: Speciation of organic fraction does matter for source apportionment. Part 1: A one-year campaign in Grenoble (France), Sci. Total Environ., 624, 1598–1611, https://doi.org/10.1016/j.scitotenv.2017.12.135, 2018b.

Srivastava, D., Vu, T. V., Tong, S., Shi, Z., and Harrison, R. M.: Formation of secondary organic aerosols from anthropogenic precursors in laboratory studies, npj Clim. Atmos. Sci., 5, 1–30, https://doi.org/10.1038/s41612-022-00238-6, 2022.

Strollo, C. M. and Ziemann, P. J.: Products and mechanism of secondary organic aerosol formation from the reaction of 3-methylfuran with OH radicals in the presence of NO_x, Atmos. Environ., 77, 534–543, https://doi.org/10.1016/j.atmosenv.2013.05.033, 2013.

Sumlin, B. J., Pandey, A., Walker, M. J., Pattison, R. S., Williams, B. J., and Chakrabarty, R. K.: Atmospheric Photooxidation Diminishes Light Absorption by Primary Brown Carbon Aerosol

from Biomass Burning, Environ. Sci. Technol. Lett., 4, 540–545, https://doi.org/10.1021/acs.estlett.7b00393, 2017.

Tajuelo, M., Rodríguez, D., Rodríguez, A., Escalona, A., Viteri, G., Aranda, A., and Diaz-de-Mera, Y.: Secondary organic aerosol formation from the ozonolysis and oh-photooxidation of 2,5-dimethylfuran, Atmos. Environ., 245, 118041, https://doi.org/10.1016/j.atmosenv.2020.118041, 2021.

Thurston, G. D., Ahn, J., Cromar, K. R., Shao, Y., Reynolds, H. R., Jerrett, M., Lim, C. C., Shanley, R., Park, Y., and Hayes, R. B.: Ambient Particulate Matter Air Pollution Exposure and Mortality in the NIH-AARP Diet and Health Cohort, Environ. Health Perspect., 124, 484–490, https://doi.org/10.1289/ehp.1509676, 2016.

Tiitta, P., Leskinen, A., Hao, L., Yli-Pirilä, P., Kortelainen, M., Grigonyte, J., Tissari, J., Lamberg, H., Hartikainen, A., Kuuspalo, K., Kortelainen, A.-M., Virtanen, A., Lehtinen, K. E. J., Komppula, M., Pieber, S., Prévôt, A. S. H., Onasch, T. B., Worsnop, D. R., Czech, H., Zimmermann, R., Jokiniemi, J., and Sippula, O.: Transformation of logwood combustion emissions in a smog chamber: formation of secondary organic aerosol and changes in the primary organic aerosol upon daytime and nighttime aging, Atmos. Chem. Phys., 16, 13251–13269, https://doi.org/10.5194/acp-16-13251-2016, 2016.

Tomaz, S., Shahpoury, P., Jaffrezo, J.-L., Lammel, G., Perraudin, E., Villenave, E., and Albinet, A.: One-year study of polycyclic aromatic compounds at an urban site in Grenoble (France): Seasonal variations, gas/particle partitioning and cancer risk estimation, Sci. Total Environ., 565, 1071–1083, https://doi.org/10.1016/j.scitotenv.2016.05.137, 2016.

Tsimpidi, A. P., Karydis, V. A., Pozzer, A., Pandis, S. N., and Lelieveld, J.: ORACLE (v1.0): module to simulate the organic aerosol composition and evolution in the atmosphere, Geosci. Model Dev., 7, 3153–3172, https://doi.org/10.5194/gmd-7-3153-2014, 2014.

Updyke, K. M., Nguyen, T. B., and Nizkorodov, S. A.: Formation of brown carbon via reactions of ammonia with secondary organic aerosols from biogenic and anthropogenic precursors, Atmos. Environ., 63, 22–31, https://doi.org/10.1016/j.atmosenv.2012.09.012, 2012.

Viana, M., Alastuey, A., Querol, X., Guerreiro, C., Vogt, M., Colette, A., Collet, S., Albinet, A., Fraboulet, I., Lacome, J.-M., Tognet, F., and De Leeuw, F.: Contribution of residential combustion to ambient air pollution and greenhouse gas emissions, European Environment Agency (EEA), https://www.eionet.europa.eu/etcs/etc-atni/products/etc-atni-reports/etcacm_tp_2015_1_residential_combustion (last access: 24 November 2023), 2016.

Vicente, E. D. and Alves, C. A.: An overview of particulate emissions from residential biomass combustion, Atmos. Res., 199, 159–185, https://doi.org/10.1016/j.atmosres.2017.08.027, 2018.

Wang, S., Ye, J., Soong, R., Wu, B., Yu, L., Simpson, A. J., and Chan, A. W. H.: Relationship between chemical composition and oxidative potential of secondary organic aerosol from polycyclic aromatic hydrocarbons, Atmos. Chem. Phys., 18, 3987–4003, https://doi.org/10.5194/acp-18-3987-2018, 2018.

Washenfelder, R. A., Attwood, A. R., Brock, C. A., Guo, H., Xu, L., Weber, R. J., Ng, N. L., Allen, H. M., Ayres, B. R., Baumann, K., Cohen, R. C., Draper, D. C., Duffey, K. C., Edgerton, E., Fry, J. L., Hu, W. W., Jimenez, J. L., Palm, B. B., Romer, P., Stone, E. A., Wooldridge, P. J., and Brown, S. S.: Biomass burning dominates brown carbon absorption in the rural southeastern United States, Geophys. Res. Lett., 42, 653–664, https://doi.org/10.1002/2014GL062444, 2015.

Weber, S., Salameh, D., Albinet, A., Alleman, L. Y., Waked, A., Besombes, J.-L., Jacob, V., Guillaud, G., Meshbah, B., Rocq, B., Hulin, A., Dominik-Sègue, M., Chrétien, E., Jaffrezo, J.-L., and Favez, O.: Comparison of PM10 Sources Profiles at 15 French Sites Using a Harmonized Constrained Positive Matrix Factorization Approach, Atmosphere, 10, 310, https://doi.org/10.3390/atmos10060310, 2019.

Xie, M., Chen, X., Hays, M. D., Lewandowski, M., Offenberg, J., Kleindienst, T. E., and Holder, A. L.: Light Absorption of Secondary Organic Aerosol: Composition and Contribution of Nitroaromatic Compounds, Environ. Sci. Technol., 51, 11607–11616, https://doi.org/10.1021/acs.est.7b03263, 2017a.

Xie, M., Hays, M. D., and Holder, A. L.: Light-absorbing organic carbon from prescribed and laboratory biomass burning and gasoline vehicle emissions, Sci. Rep., 7, 7318, https://doi.org/10.1038/s41598-017-06981-8, 2017b.

Xu, W., Croteau, P., Williams, L., Canagaratna, M., Onasch, T., Cross, E., Zhang, X., Robinson, W., Worsnop, D., and Jayne, J.: Laboratory characterization of an aerosol chemical speciation monitor with $PM_{2.5}$ measurement capability, Aerosol Sci. Technol., 51, 69–83, https://doi.org/10.1080/02786826.2016.1241859, 2017.

Yee, L. D., Kautzman, K. E., Loza, C. L., Schilling, K. A., Coggon, M. M., Chhabra, P. S., Chan, M. N., Chan, A. W. H., Hersey, S. P., Crounse, J. D., Wennberg, P. O., Flagan, R. C., and Seinfeld, J. H.: Secondary organic aerosol formation from biomass burning intermediates: phenol and methoxyphenols, Atmos. Chem. Phys., 13, 8019–8043, https://doi.org/10.5194/acp-13-8019-2013, 2013.

Zhang, Q., Jimenez, J. L., Canagaratna, M. R., Allan, J. D., Coe, H., Ulbrich, I., Alfarra, M. R., Takami, A., Middlebrook, A. M., Sun, Y. L., Dzepina, K., Dunlea, E., Docherty, K., DeCarlo, P. F., Salcedo, D., Onasch, T., Jayne, J. T., Miyoshi, T., Shimono, A., Hatakeyama, S., Takegawa, N., Kondo, Y., Schneider, J., Drewnick, F., Borrmann, S., Weimer, S., Demerjian, K., Williams, P., Bower, K., Bahreini, R., Cottrell, L., Griffin, R. J., Rautiainen, J., Sun, J. Y., Zhang, Y. M., and Worsnop, D. R.: Ubiquity and dominance of oxygenated species in organic aerosols in anthropogenically-influenced Northern Hemisphere midlatitudes, Geophys. Res. Lett., 34, L13801, https://doi.org/10.1029/2007GL029979, 2007.

Zhang, Q., Jimenez, J. L., Canagaratna, M. R., Ulbrich, I. M., Ng, N. L., Worsnop, D. R., and Sun, Y.: Understanding atmospheric organic aerosols via factor analysis of aerosol mass spectrometry: a review, Anal. Bioanal. Chem., 401, 3045–3067, https://doi.org/10.1007/s00216-011-5355-y, 2011.

Zhang, X., Kim, H., Parworth, C. L., Young, D. E., Zhang, Q., Metcalf, A. R., and Cappa, C. D.: Optical Properties of Wintertime Aerosols from Residential Wood Burning in Fresno, CA: Results from DISCOVER-AQ 2013, Environ. Sci. Technol., 50, 1681–1690, https://doi.org/10.1021/acs.est.5b04134, 2016.

Zhang, Y., Favez, O., Canonaco, F., Liu, D., Moènik, G., Amodeo, T., Sciare, J., Prévôt, A. S. H., Gros, V., and Albinet, A.: Evidence of major secondary organic aerosol contribution to lensing

effect black carbon absorption enhancement, npj Clim. Atmos. Sci., 1, 47, https://doi.org/10.1038/s41612-018-0056-2, 2018.

Zhang, Y., Favez, O., Petit, J.-E., Canonaco, F., Truong, F., Bonnaire, N., Crenn, V., Amodeo, T., Prévôt, A. S. H., Sciare, J., Gros, V., and Albinet, A.: Six-year source apportionment of submicron organic aerosols from near-continuous highly time-resolved measurements at SIRTA (Paris area, France), Atmos. Chem. Phys., 19, 14755–14776, https://doi.org/10.5194/acp-19-14755-2019, 2019.

Zhang, Y., Albinet, A., Petit, J.-E., Jacob, V., Chevrier, F., Gille, G., Pontet, S., Chrétien, E., Dominik-Sègue, M., Levigoureux, G., Moènik, G., Gros, V., Jaffrezo, J.-L., and Favez, O.: Substantial brown carbon emissions from wintertime residential wood burning over France, Sci. Total Environ., 743, 140752, https://doi.org/10.1016/j.scitotenv.2020.140752, 2020.

Zhang, Y., Sun, J., Zou, H., Zhang, B., Yang, D., Wang, Q., Li, J., Qu, L., Ho, S. S. H., Cao, J., and Shen, Z.: Photochemical aging process on PM2.5 bound PAHs emission from solid fuel combustion in traditional and improved stoves, Atmos. Res., 263, 105807, https://doi.org/10.1016/j.atmosres.2021.105807, 2021.

Zhang, Y., Cheng, M., Gao, J., and Li, J.: Review of the influencing factors of secondary organic aerosol formation and aging mechanism based on photochemical smog chamber simulation methods, J. Environ. Sci., 123, 545–559, https://doi.org/10.1016/j.jes.2022.10.033, 2023.

Zheng, H.-Y., Zhu, Y.-L., Teng, B.-T., Bai, Z.-Q., Zhang, C.-H., Xiang, H.-W., and Li, Y.-W.: Towards understanding the reaction pathway in vapour phase hydrogenation of furfural to 2-methylfuran, J. Mol. Catal. A-Chem., 246, 18–23, https://doi.org/10.1016/j.molcata.2005.10.003, 2006.

Zhou, S. and Wenger, J. C.: Kinetics and products of the gas-phase reactions of acenaphthene with hydroxyl radicals, nitrate radicals and ozone, Atmos. Environ., 72, 97–104, https://doi.org/10.1016/j.atmosenv.2013.02.044, 2013a.

Zhou, S. and Wenger, J. C.: Kinetics and products of the gas-phase reactions of acenaphthylene with hydroxyl radicals, nitrate radicals and ozone, Atmos. Environ., 75, 103–112, https://doi.org/10.1016/j.atmosenv.2013.04.049, 2013b.

Zielinska, B.: Analysis of Semi-Volatile Organic Compound by GC/MS, DRI Standard Operating Procedure, Desert Research Institute, Reno (NV), http://www.epa.gov/ttnamti1/files/ambient/pm25/spec/DRISOPSVOC92408.pdf (last access: 24 November 2023), 2008.

Ziemann, P. J. and Atkinson, R.: Kinetics, products, and mechanisms of secondary organic aerosol formation, Chem. Soc. Rev., 41, 6582, https://doi.org/10.1039/c2cs35122f, 2012.